A COMPLEX PERMITTIVITY AND PERMEABILITY MEASUREMENT SYSTEM FOR ELEVATED TEMPERATURES

Final Report
December, 1989 - July 1990

Grant No. NAG 3-972

Submitted to:

NASA Lewis Research Center
Attn: Mr. Carl A. Stearns
21000 Brookpark Road
Mail Stop 106-1
Cleveland, Ohio 44135

Submitted by:

Georgia Institute of Technology
Georgia Tech Research Institute
Electronics and Computer Systems Laboratory
Electromagnetic Effectiveness Division
Atlanta, Georgia 30332-0800
Principal Investigator: Paul Friederich

Contracting through:

Georgia Tech Research Corporation
Centennial Research Building
Atlanta, Georgia 30332-0420

GEORGIA INSTITUTE OF TECHNOLOGY
A Unit of the University System of Georgia
Atlanta, Georgia 30332

GTRI
GEORGIA TECH RESEARCH INSTITUTE

A COMPLEX PERMITTIVITY AND PERMEABILITY MEASUREMENT SYSTEM FOR ELEVATED TEMPERATURES

Final Report
December, 1989 - July 1990

Grant No. NAG 3-972

Submitted to:

NASA Lewis Research Center
Attn: Mr. Carl A. Stearns
21000 Brookpark Road
Mail Stop 106-1
Cleveland, Ohio 44135

Submitted by:

Georgia Institute of Technology
Georgia Tech Research Institute
Electronics and Computer Systems Laboratory
Electromagnetic Effectiveness Division
Atlanta, Georgia 30332-0800
Principal Investigator: Paul Friederich

Contracting through:

Georgia Tech Research Corporation
Centennial Research Building
Atlanta, Georgia 30332-0420

Table of Contents

List of Figures

List of Tables

I. Introduction

This research has been supported by Grant No. NAG 3-972 from NASA Lewis Research Center (LeRC). The technical monitor is Mr. C. A. Stearns of the Environmental Durability Branch. The goals of this research program are threefold: 1) To fully develop a method to measure the permittivity and permeability of special materials as a function of frequency in the range of 2.6 to 18 GHz, and of temperature in the range of 25 to 1100° C; 2) To assist LeRC in setting up an in-house system for the measurement of high-temperature permittivity and permeability; 3) To measure the complex permittivity and permeability of special materials as a function of frequency and temperature to demonstrate the capability of the method. Significant contributions toward these goals have been made by GTRI personnel Dr. Rick Moore and Tanya Robbins.

II. Project Progress

A. Background

The method chosen for characterizing the sponsor-furnished materials is based on standards issued by the American Society for Testing and Materials (ASTM), standards D 2520-86 [1] (Complex Permittivity of Solid Electrical Insulating Materials at Microwave Frequencies and Temperatures to 1650°C) and F 131-70 [2] (Complex Dielectric Constant of Nonmetallic Magnetic Materials at Microwave Frequencies). This method relies on perturbation of a resonant cavity with a small volume of sample material. Different field configurations in the cavity can be used to separate electric and magnetic effects. Moore, et al. presented a detailed explanation of this technique, with particular emphasis on applications with anisotropic ferrites, in a paper which appeared in the American Institute of Physics (AIP) Review of Scientific Instruments [3].

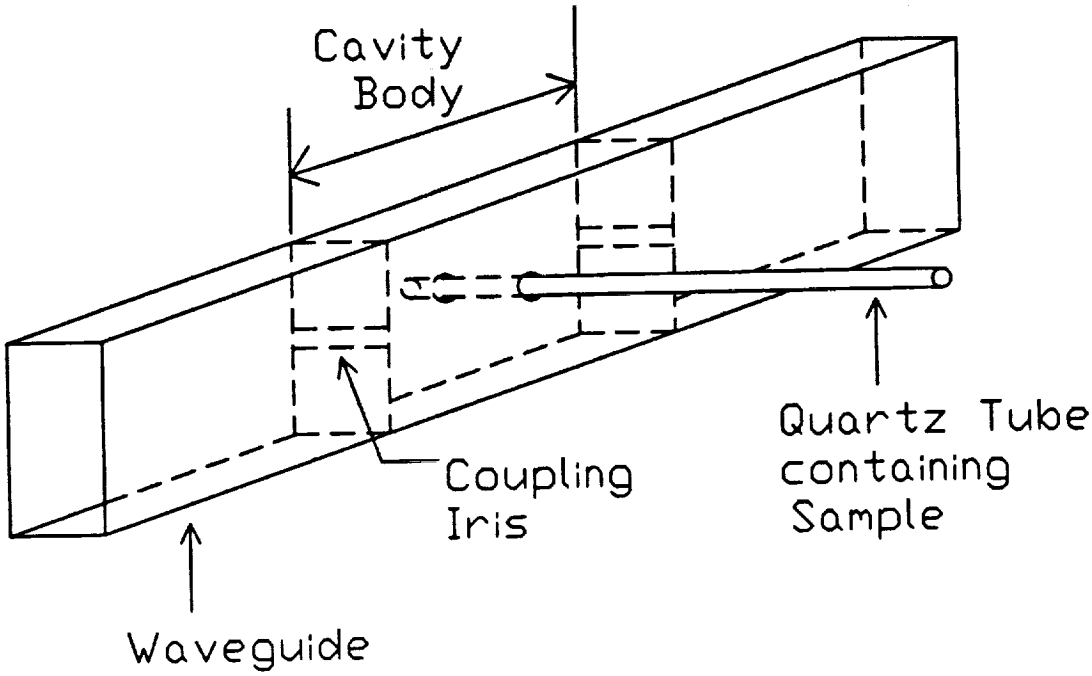

Figure 1. Diagram showing configuration of rectangular waveguide cavity used for measurements. The illustrated orientation of the sample would be used with odd modes for permittivity measurements. For permeability measurements, the sample would be inserted parallel to the broad wall.

Figure 1 illustrates the physical configuration of the waveguide cavity and sample. The cavity consists of a section of rectangular waveguide terminated at each end with a vertical slot iris. In the center of one wall is a small hole through which the sample is introduced. For permittivity measurements the hole is in the center of the broad wall, and an odd resonance mode (i.e., TE_{10n}, with n odd) is used. The sample is thus located at a point of maximum electric field, and for small sample volumes the field is nearly constant over the sample region. Similarly, for permeability measurements the sample hole is located in the middle of the narrow wall and an even resonance mode is used. Thus, the sample is at a point of maximum magnetic field.

Typically, the sample is contained in a small bore quartz tube. Such tubes have been used with powdered samples, fiber samples, and thin ceramic rods. A calibration measurement for such a sample would include measurement of the cavity with an empty quartz tube in place, so that perturbation effects could be solely attributed to the sample.

B. Cavity Design

Drawings of a waveguide cavity for use at X band have been furnished separately to LeRC. Cavities for other bands are similar except for size. Key features of the cavity design include the location of sample holes as explained above; the material from which the assembly is fabricated; the length of the cavity; and the location of the joint between pieces. The assembly is fabricated from Hastelloy, an alloy of nickel developed to withstand temperatures in excess of 1200° C. Cavity lengths are designed to support three modes of the form TE_{10n}, so that each cavity will have either two odd modes and one even, or two even modes and one odd. It is expected that the complete system will include two cavities, one of each type, in each band. Those cavities with two odd modes can be joined at a seam through the narrow walls, while those cavities with two even modes can be joined at a seam through the broad walls. Location of the seam in the narrow wall will minimize its effect on permittivity measurements, while a seam in the broad wall is best for permeability measurements. Table I shows possible cavity lengths for each waveguide band, along with the in-band resonant modes which would be expected for each length. The width and height of each cavity are assumed to be the dimensions of the standard rectangular waveguide for each band, i.e., WR-187 for C band, WR-137 for Xn band, WR-90 for X band, and WR-62 for Ku band.

TABLE I

RESONANT MODE VS FREQUENCY (GHZ) FOR VARIOUS LENGTHS

Mode: TE_{102}	TE_{103}	TE_{104}	TE_{105}	TE_{106}	
C band					
6.6"		4.1393	4.7676	5.47046	
4.8"	3.9980	4.8520	5.8415		
Xn band					
4.3"		5.9543	6.9741	8.0988	
5.5"			6.0764	6.8763	7.7426
X band					
3.3"		8.4722	9.7039	11.0882	
3.8"			9.0325	10.1633	11.3939
Ku band					
2.1"		12.692	14.710	16.954	
2.6"			13.132	14.792	16.598

C. Room Temperature Measurements

The third goal of this program is to demonstrate the capabilities of this method by applying it to special samples provided by NASA Lewis. Eight samples were sent in the initial batch, five of which arrived intact. The other three were broken and mixed together. We were unable to distinguish the pieces by composition and reunite them into measurable samples, so they will be put aside and returned to NASA after the other samples are measured. These samples have been labelled Batch 1. Two other batches have also been received, under the designations 60-1015 and 60-1520. They will be referred to as batches 2 and 3, respectively. All unbroken samples in the three batches have been measured at room temperature.

Room temperature measurements were performed in waveguide cavities which were either made of copper (C and Xn bands) or gold-plated (X and Ku bands). These materials provide a higher conductivity and, consequently, better quality factor in the cavities than the nickel which is required for higher temperatures. A higher quality factor makes smaller changes distinguishable, and thus makes the measurements more

sensitive. The results of these room temperature measurements were presented in detail in the semi-annual status report for the period July-December, 1989. Table 2 is a summary of the dielectric properties obtained from those measurements, where the average was taken over five to eight samples in each batch, four frequency bands, up to four frequencies in each band, and two measurements at each frequency. As explained in that status report, these averages include the effects of inhomogeneities in the samples themselves since the measurements were collected at different regions along each sample.

Figures 2-4 summarize the corresponding data collected at room temperature for the permeability values. Since the permeability is very likely to change with frequency in this region, the averages have been presented as plots versus frequency. The averages at each frequency point were taken over all samples in a batch and two measurements at each frequency. Since different regions of each sample were measured in successive measurements, the standard deviation lines include the effects of inhomogeneities in the samples. Also, the same regions were not necessarily measured in each band, so different band segments in the plots do not necessarily represent averages of the same measured regions.

TABLE 2
AVERAGE DIELECTRIC VALUES FOR EACH SAMPLE BATCH

Batch	Average Dielectric Constant	Standard Deviation	Average Loss Tangent	Standard Deviation
1	9.72	.73	.0088	.0022
2	8.58	1.05	.0065	.0023
3	8.55	.58	.0073	.0023

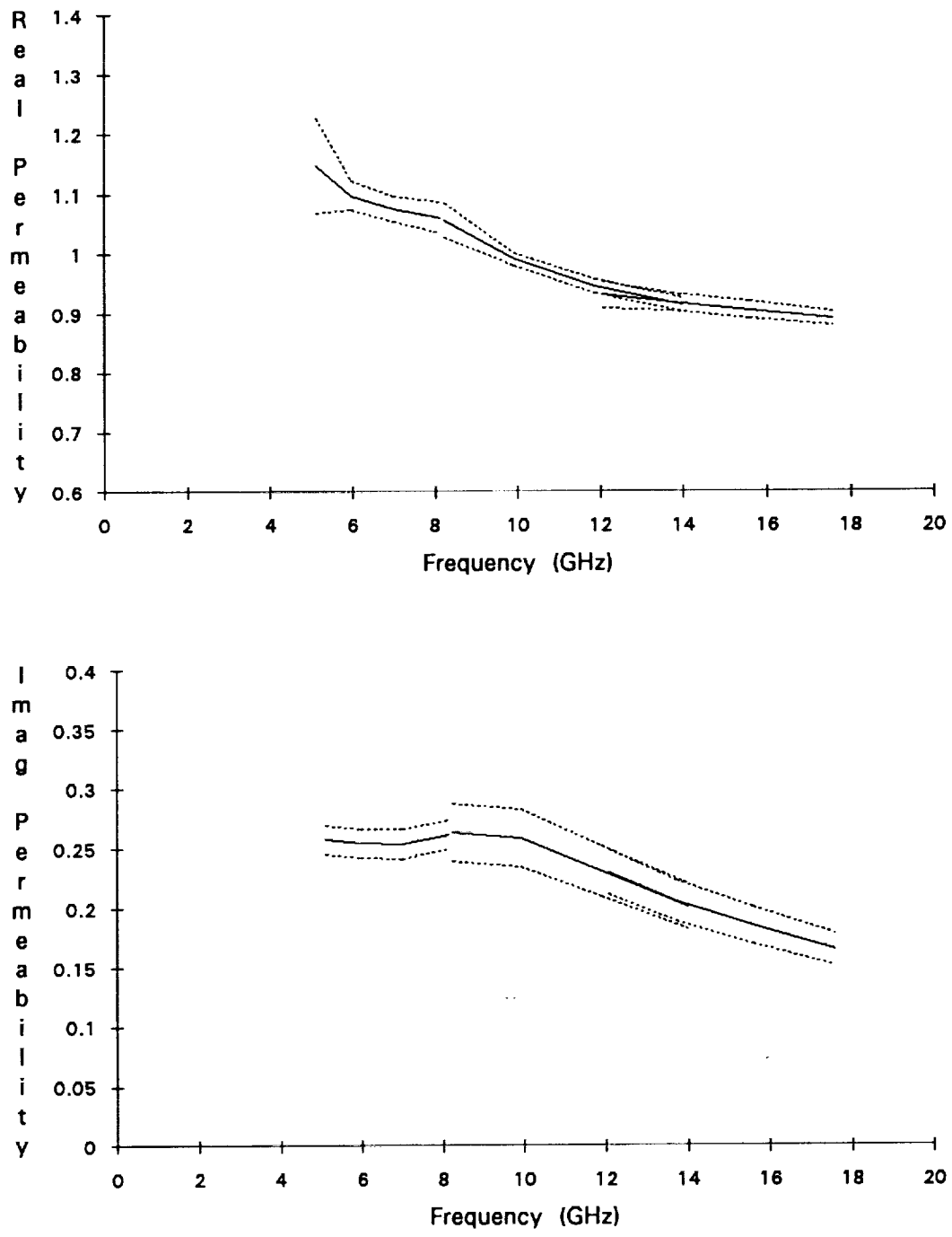

Figure 2. Average values plus and minus one standard deviation for samples in batch 1. Each segment represents results from one waveguide cavity (one band).

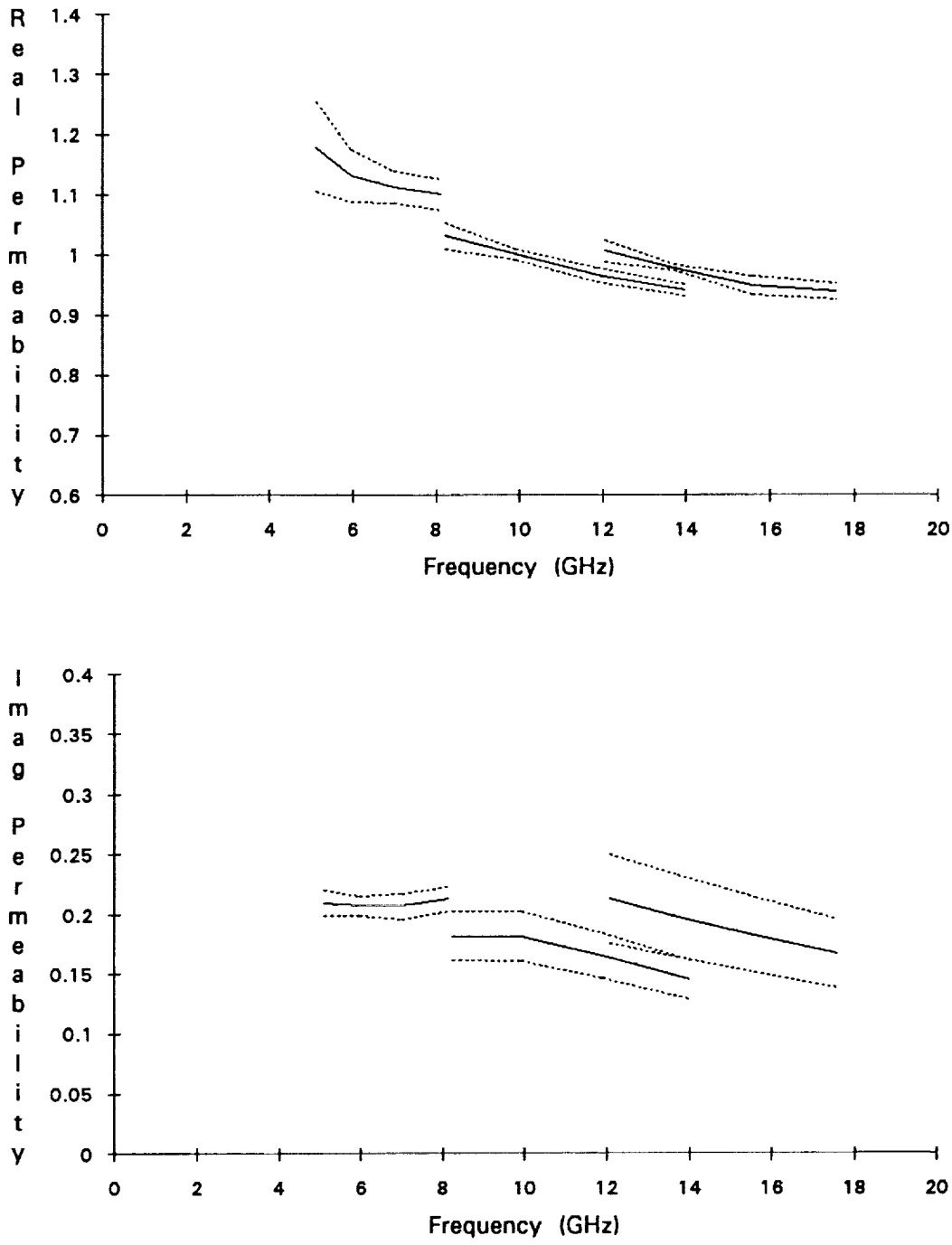

Figure 3. Average values plus and minus one standard deviation for samples in batch 2. Each segment represents results from one waveguide cavity (one band).

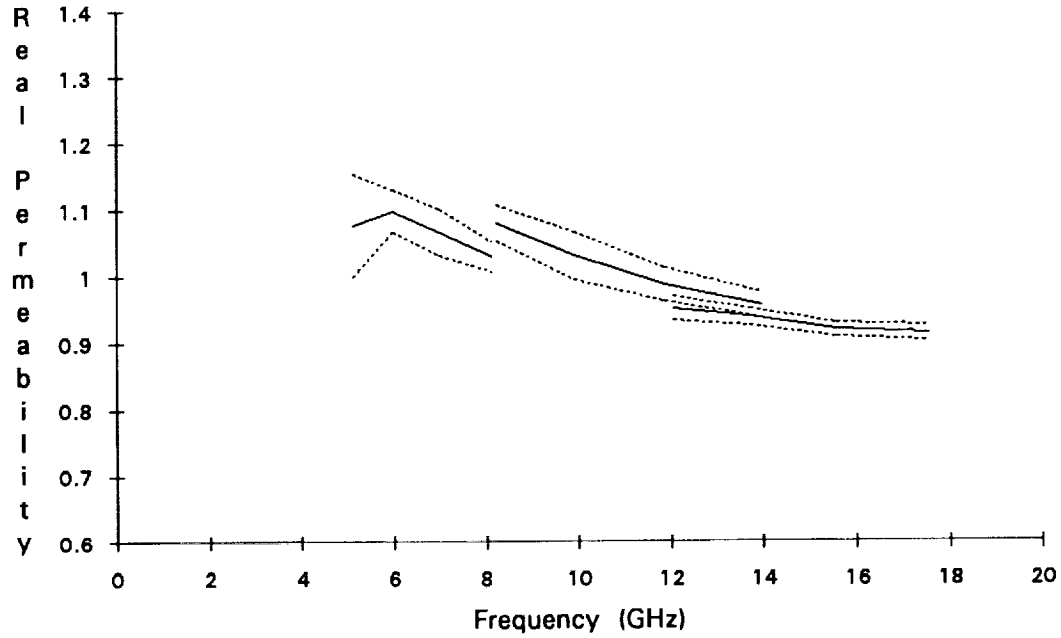

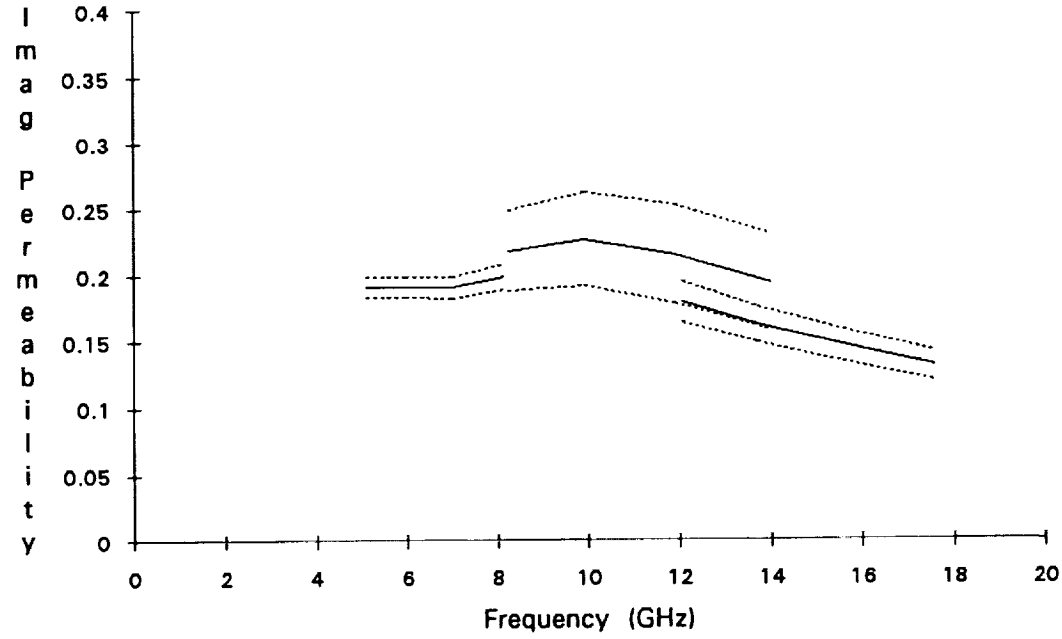

Figure 4. Average values plus and minus one standard deviation for samples in batch 3. Each segment represents results from one waveguide cavity (one band).

D. High Temperature Measurements

The high temperature measurements were performed in nickel waveguide cavities. Data was collected at temperatures of 25, 38, 149, 260, 371, 482, 593, 704, and 816°C, which correspond to Fahrenheit temperatures of 77, 100, 300, 500, 700, 900, 1100, 1300, and 1500°, respectively. Except for the fact that the cavities were located inside a clamshell furnace, the measurement procedure was the same for the high temperature case as for the room temperature case. Each sample-bearing quartz tube was introduced into the cavity through a nickel tube which extended outside the furnace. Each sample was inserted in the furnace for about 30 seconds and allowed to heat up, after which it was measured at each resonant point, a process which took about two minutes. Thus, even at the end of each heating cycle, the samples had been exposed to heat for only very short periods of time.

The order in which the waveguide cavities were used is significant. The first heating cycle occurred during the Ku band measurements; the second during the X band measurements; the third during the Xn band measurements; and the fourth during the C band measurements. The engineer performing the measurements noticed a yellow deposit forming inside the quartz tubes with many of the samples, especially in batches 1 and 3. As the temperature to which the samples were exposed increased, the deposit turned brown and the samples themselves, including some in batch 2, began to blacken. The deposits were first noticed at temperatures of 260 and 371°C, while the samples began to blacken at 371 and 482°C. This was indicative of physical changes occurring in the samples, and indeed, the dielectric properties began to show effects of these changes between 593 and 704°C. Figures 5-7 show average dielectric constant values as a function of temperature for samples in batches 1, 2, and 3, respectively. A set of data points was plotted for each waveguide band, with the average at each point including all samples in a batch (5 to 8 samples typical), all frequency points in the band (2 or 3 typical), and all measurements at each frequency (2 to 4 typical). The trend among all three batches was for the dielectric constant to show a basically flat response to the temperature increase at Ku band (first heating cycle) until the 704° measurement, at which time it began to increase dramatically to values in the 20 to 30 range. During the second heating cycle (at X band) the properties continued to vary over a wide range. However, by the third and fourth heating cycles, the average properties had become much more consistent, with a slight temperature dependence. Values measured in batch 1 ranged from 15 at room temperature up to around 23 at

816°C. For batches 2 and 3, the average values ranged from 11 at room temperature to 17 and 22, respectively, at 816°C.

Average loss tangent values are presented in Figures 8-10. They show similar heating effects to the dielectric constant values. In all three batches, the samples are much lossier after heating, probably due to carbonization from the sample matrix burning. The sample properties again exhibit more consistency by the third heating cycle, with values showing a slight rise with temperature, from 0.4 to 0.7 in batch 1, from .2 to .7 in batch 2, and from .2 to .5 in batch 3.

Figures 11-13 show average values for the real part of the sample permeability. Effects of the heating cycles are not evident in these plots, nor is there any obvious temperature dependence for the most part. However, the values in all four bands appear to converge near 1 when the temperature reaches 816 degrees, suggesting that the Curie temperature lies between 704 and 816°C. These plots do indicate a frequency dependence, with the relative permeability decreasing with increasing frequency, as one would expect.

Finally, Figures 14-16 show corresponding plots for the imaginary part of the permeability. These plots illustrate clearly that the Curie Temperature for these materials lies between 704 and 816°C, where the imaginary part approaches zero. At temperatures below 700 the materials show relatively flat temperature dependence for the imaginary part. There is a pronounced frequency dependence, however, with the imaginary part peaking in X band.

The same data sets have been plotted in Figures 17-28 vs. frequency to better reveal frequency dependent characteristics. The plots of dielectric constant in Figures 17-19 show the relatively scattered values in X and Ku bands which were symptomatic of physical changes in the samples during the first two heating cycles, perhaps decomposition of a polymer matrix. Again, the lower frequency values in Xn and C band which were obtained during later heating cycles show more consistent results and more pronounced temperature dependence. Similar results appear in Figures 20-22 with the loss tangent plots.

Figures 23-25 show the real part of the permeability vs. frequency for various temperature curves with little discernible dependence on temperature. Here the downward slope with frequency is more evident, especially in X band and below. The plots of the imaginary part of permeability in Figures 26-28 show a peak in the values at X band and an evident Curie temperature between 704 and 816°C.

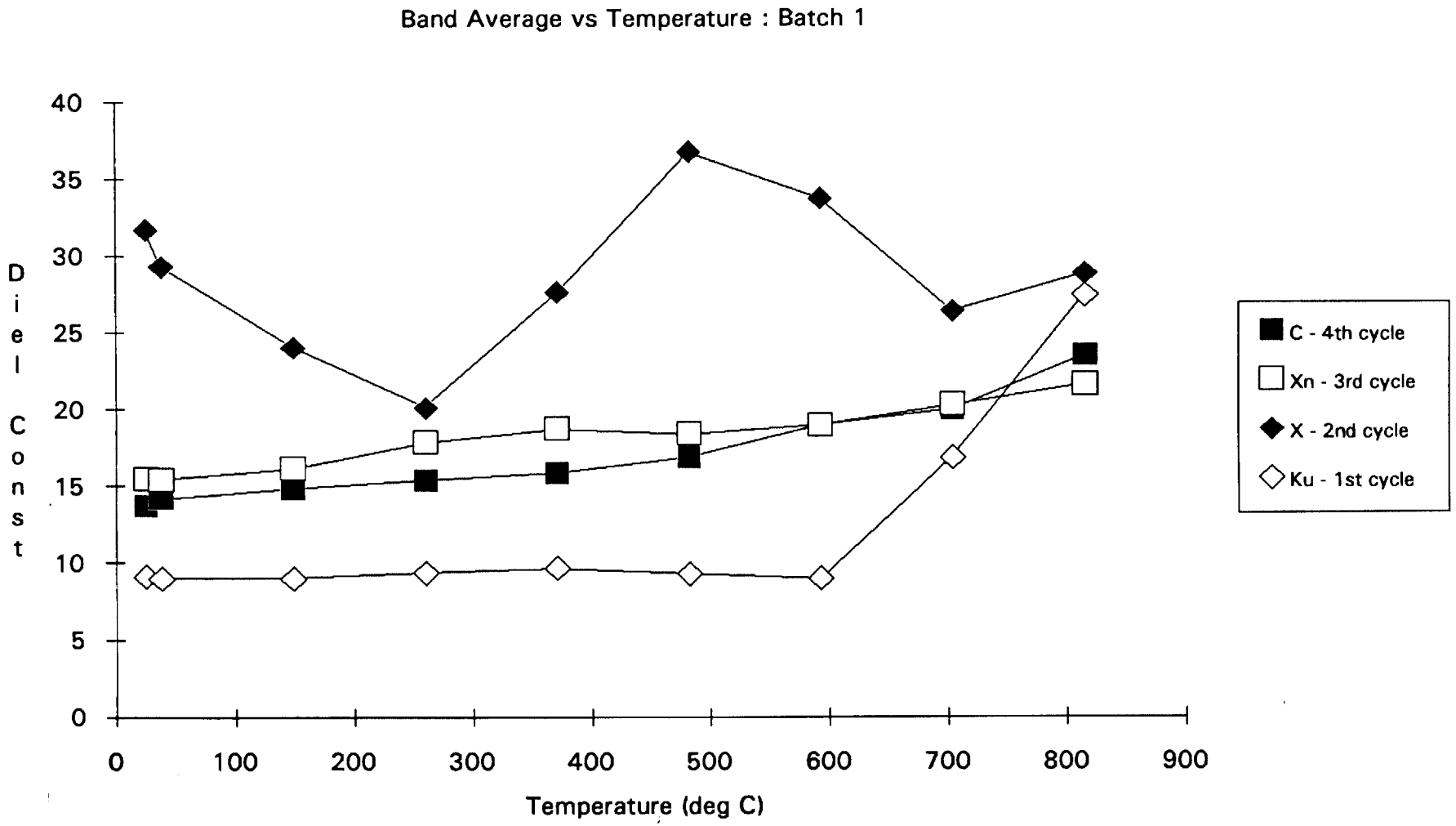

Figure 5. Average measured values for the dielectric constant of samples in batch 1 through each of four heating cycles. Differences between bands are most likely due to physical changes in the sample.

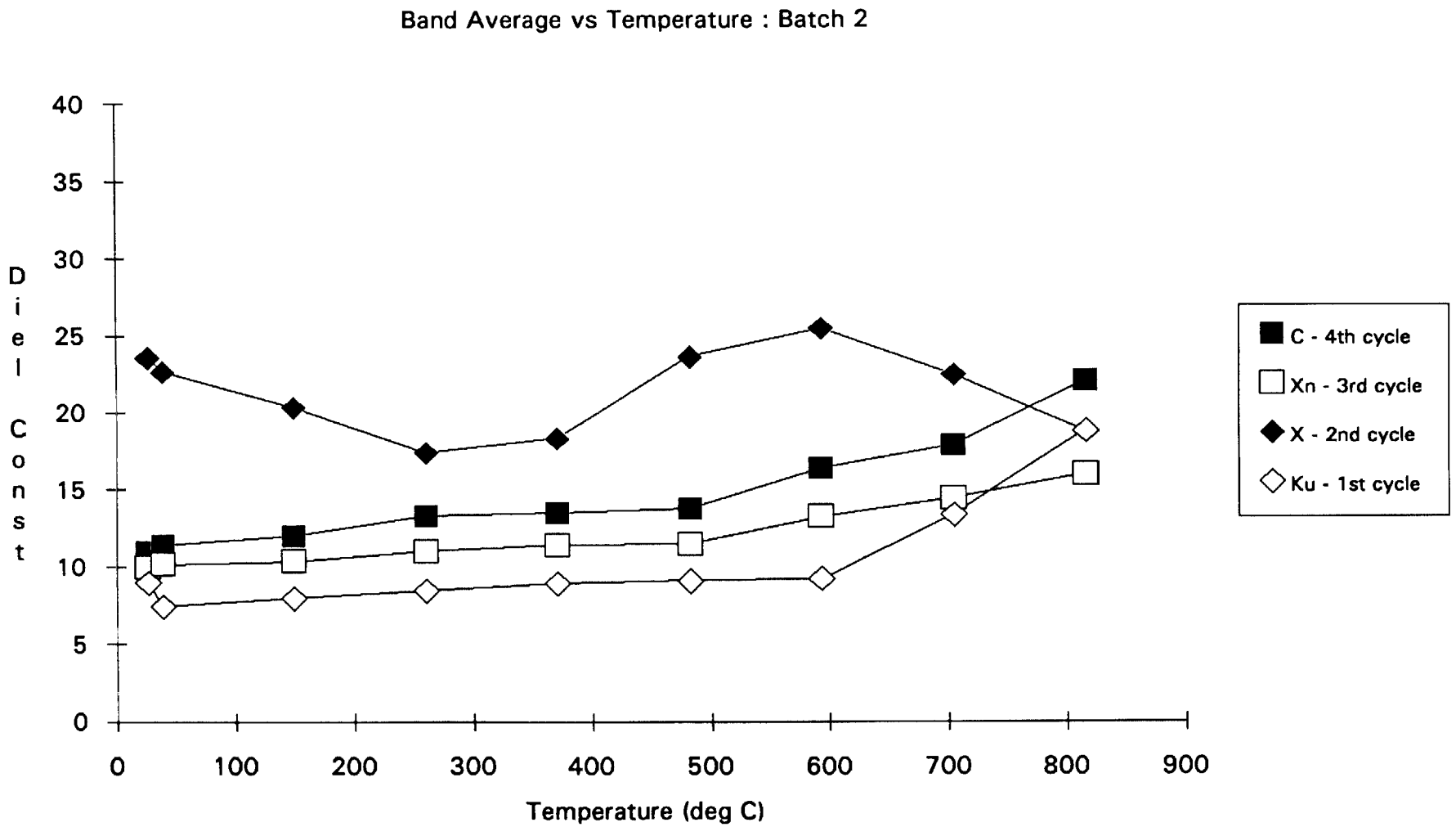

Figure 6. Average measured values for the dielectric constant of samples in batch 2 through each of four heating cycles. Differences between bands are most likely due to physical changes in the sample.

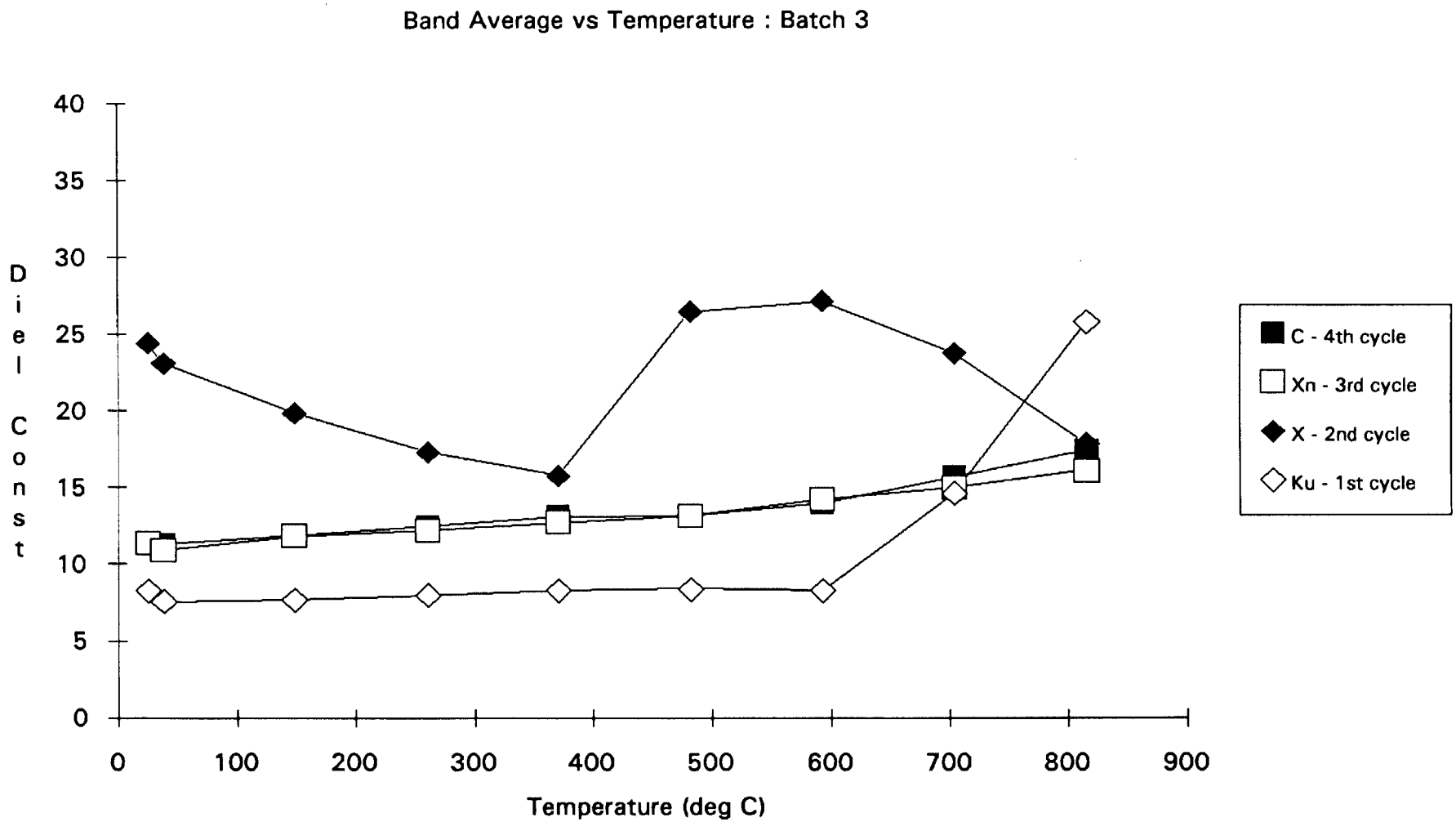

Figure 7. Average measured values for the dielectric constant of samples in batch 3 through each of four heating cycles. Differences between bands are most likely due to physical changes in the sample.

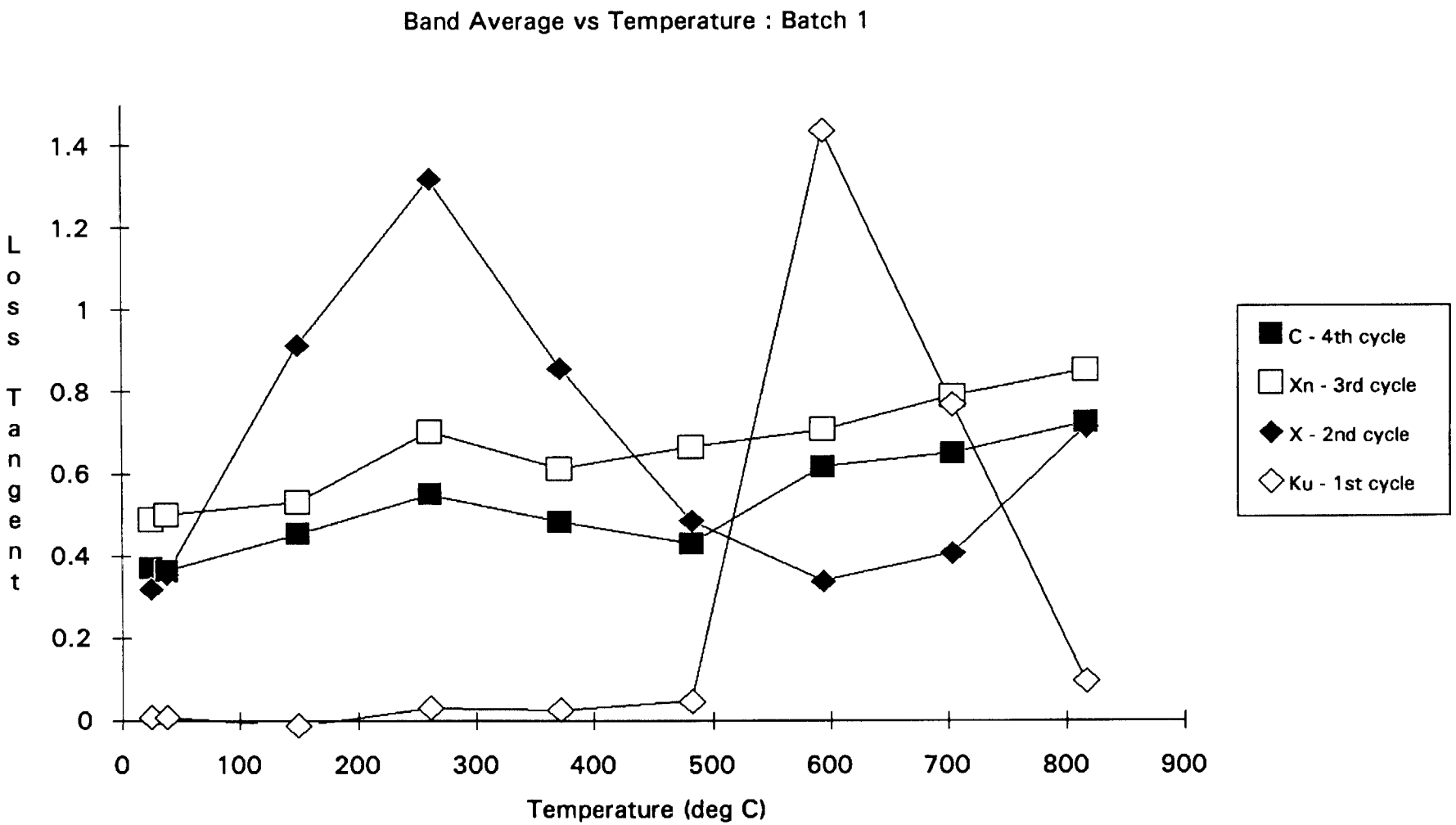

Figure 8. Average measured values for the loss tangent of samples in batch 1 through each of four heating cycles. Differences between bands are most likely due to physical changes in the sample.

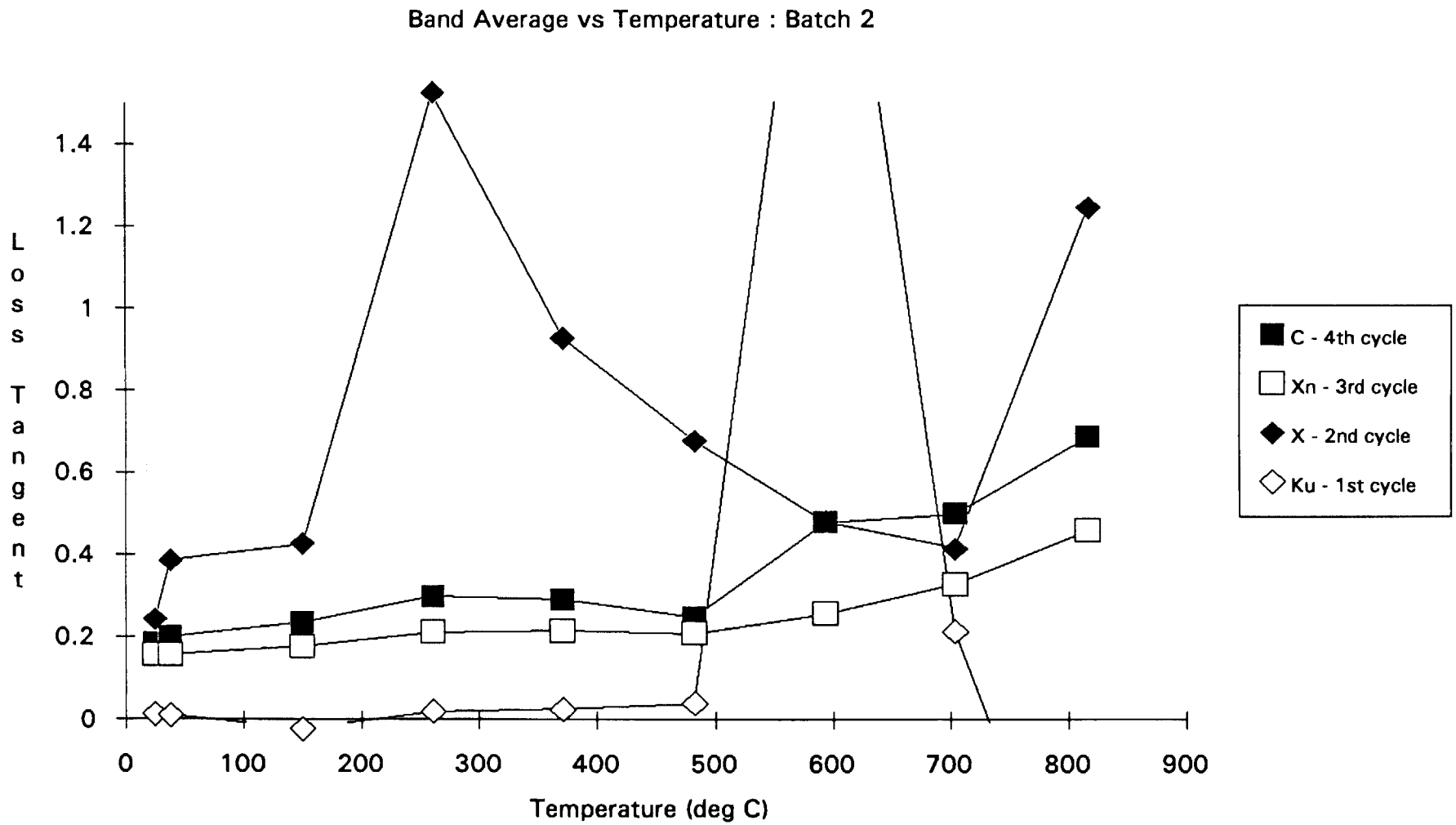

Figure 9. Average measured values for the loss tangent of samples in batch 2 through each of four heating cycles. Differences between bands are most likely due to physical changes in the sample.

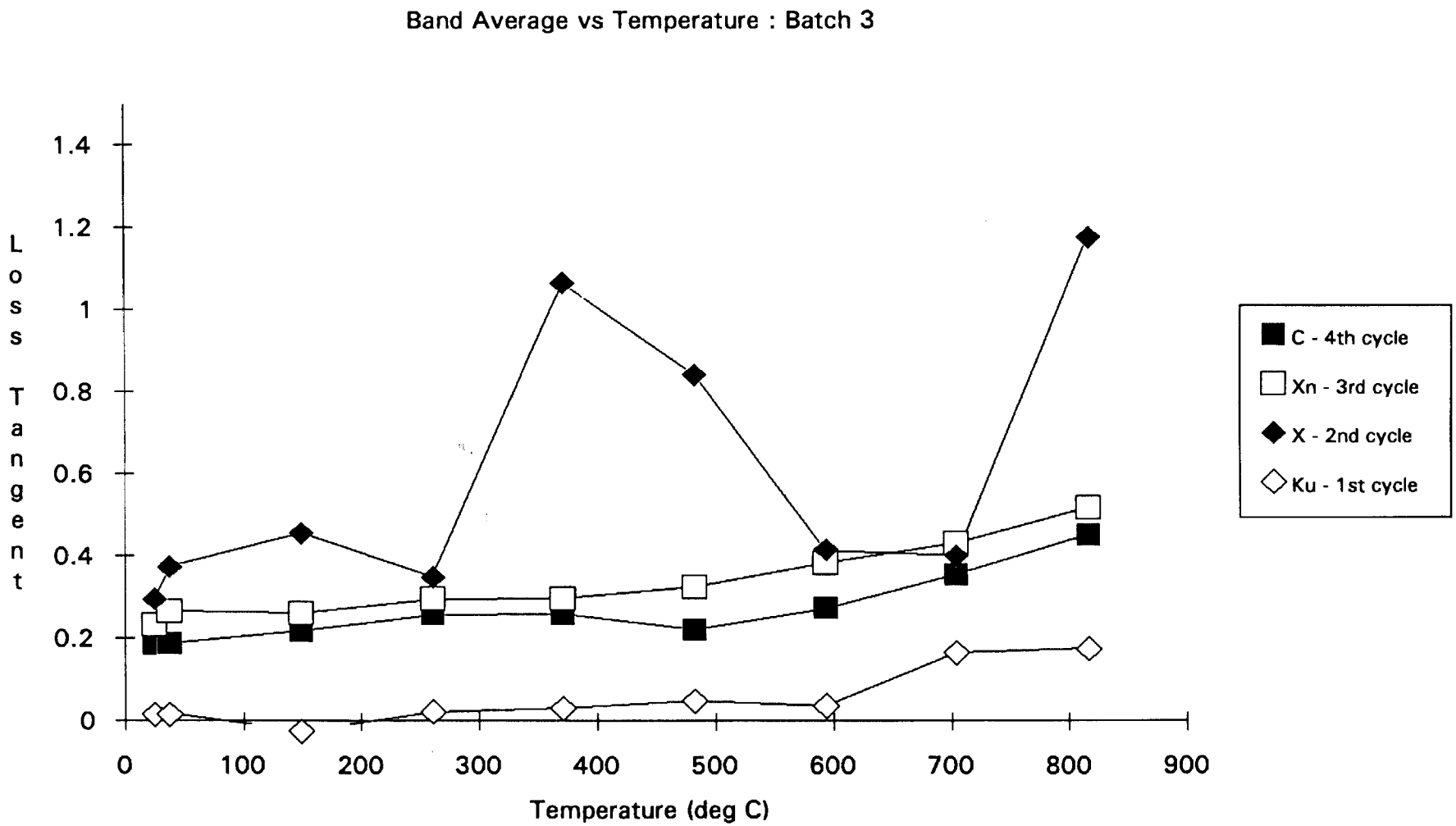

Figure 10. Average measured values for the loss tangent of samples in batch 3 through each of four heating cycles. Differences between bands are most likely due to physical changes in the sample.

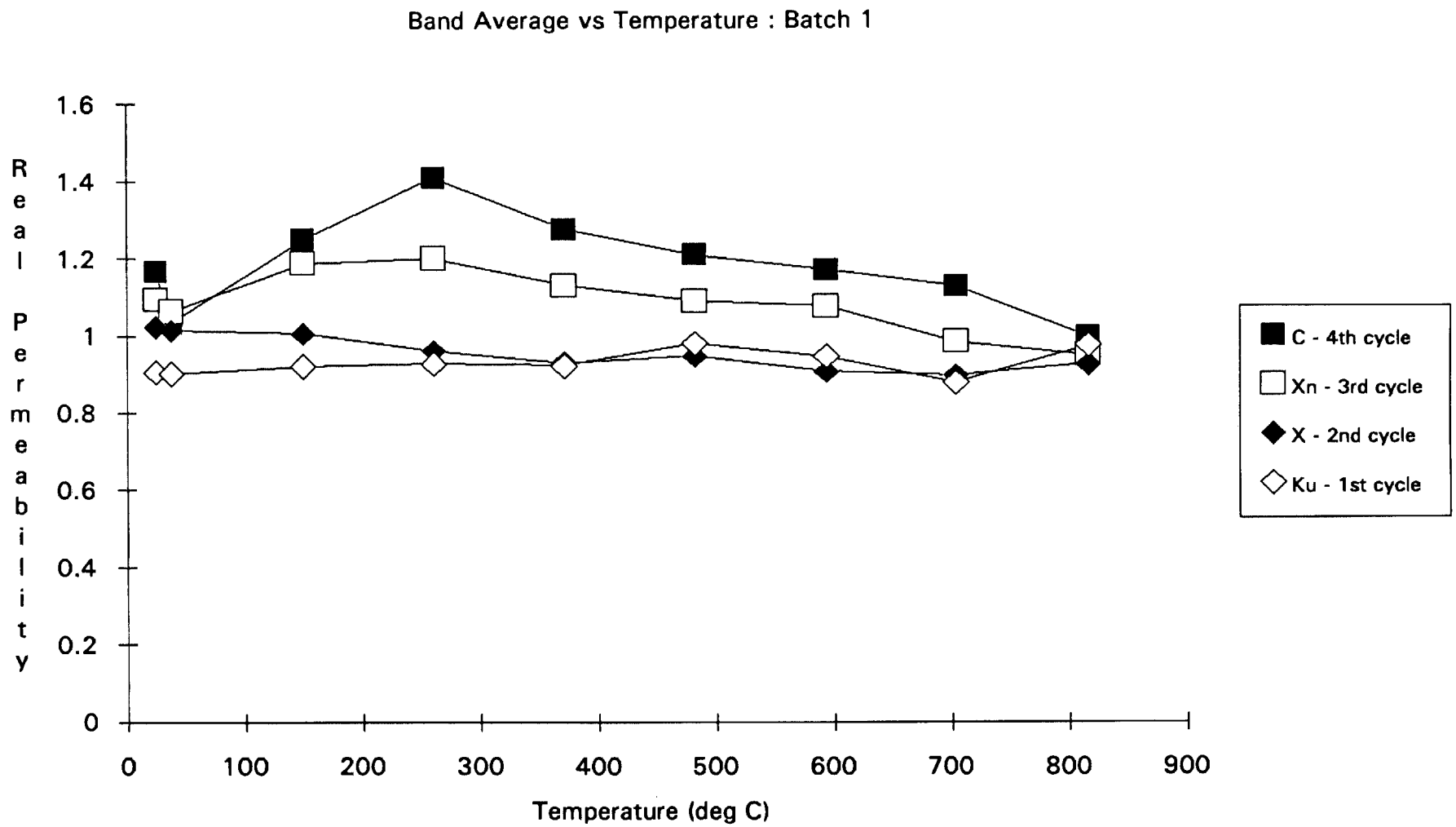

Figure 11. Average measured values for the real permeability of samples in batch 1 through each of four heating cycles. Note all four bands converge to a value near 1 as the temperature approaches 800°C.

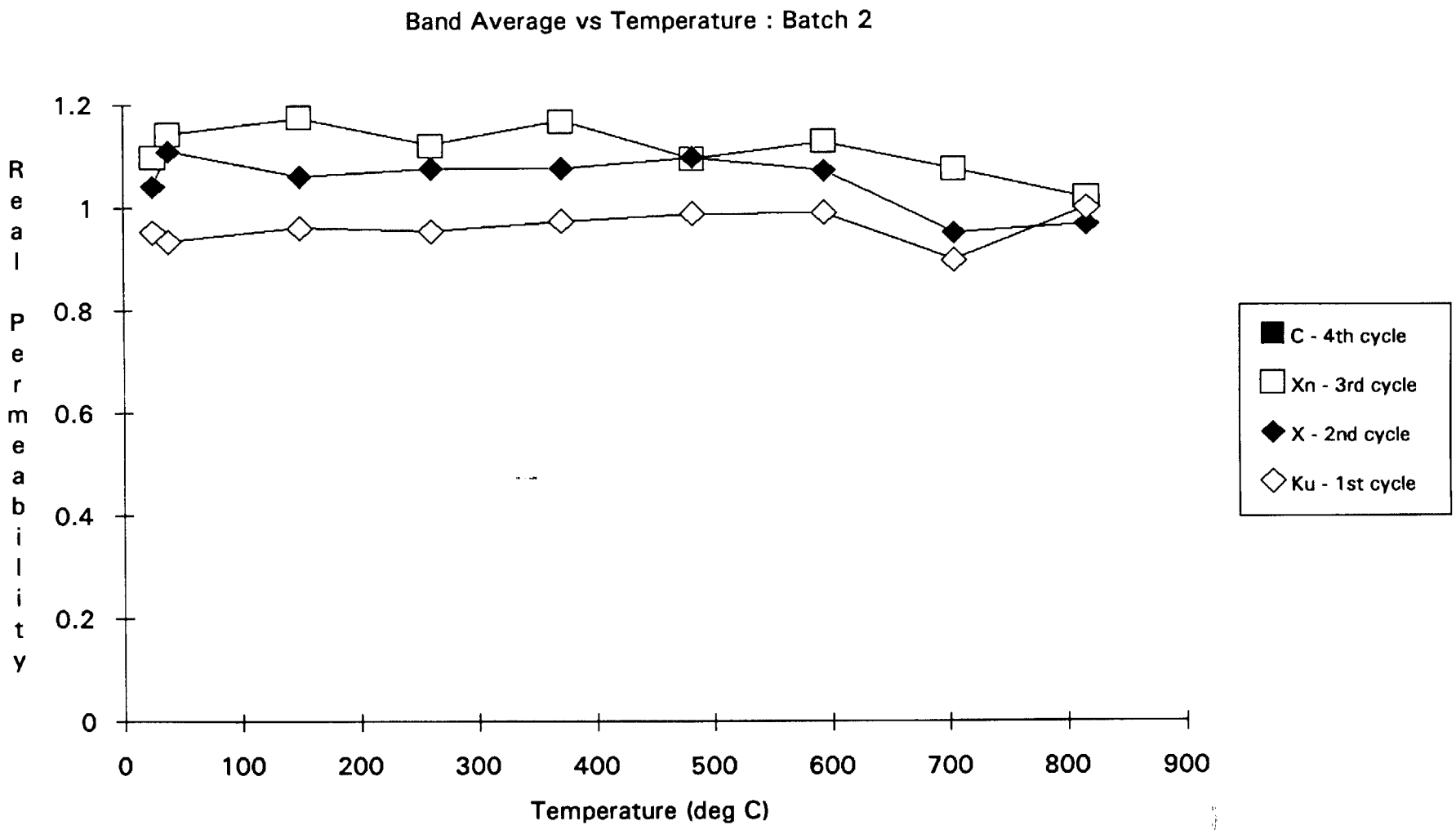

Figure 12. Average measured values for the real permeability of samples in batch 2 through each of four heating cycles. Note all four bands converge to a value near 1 as the temperature approaches 800°C.

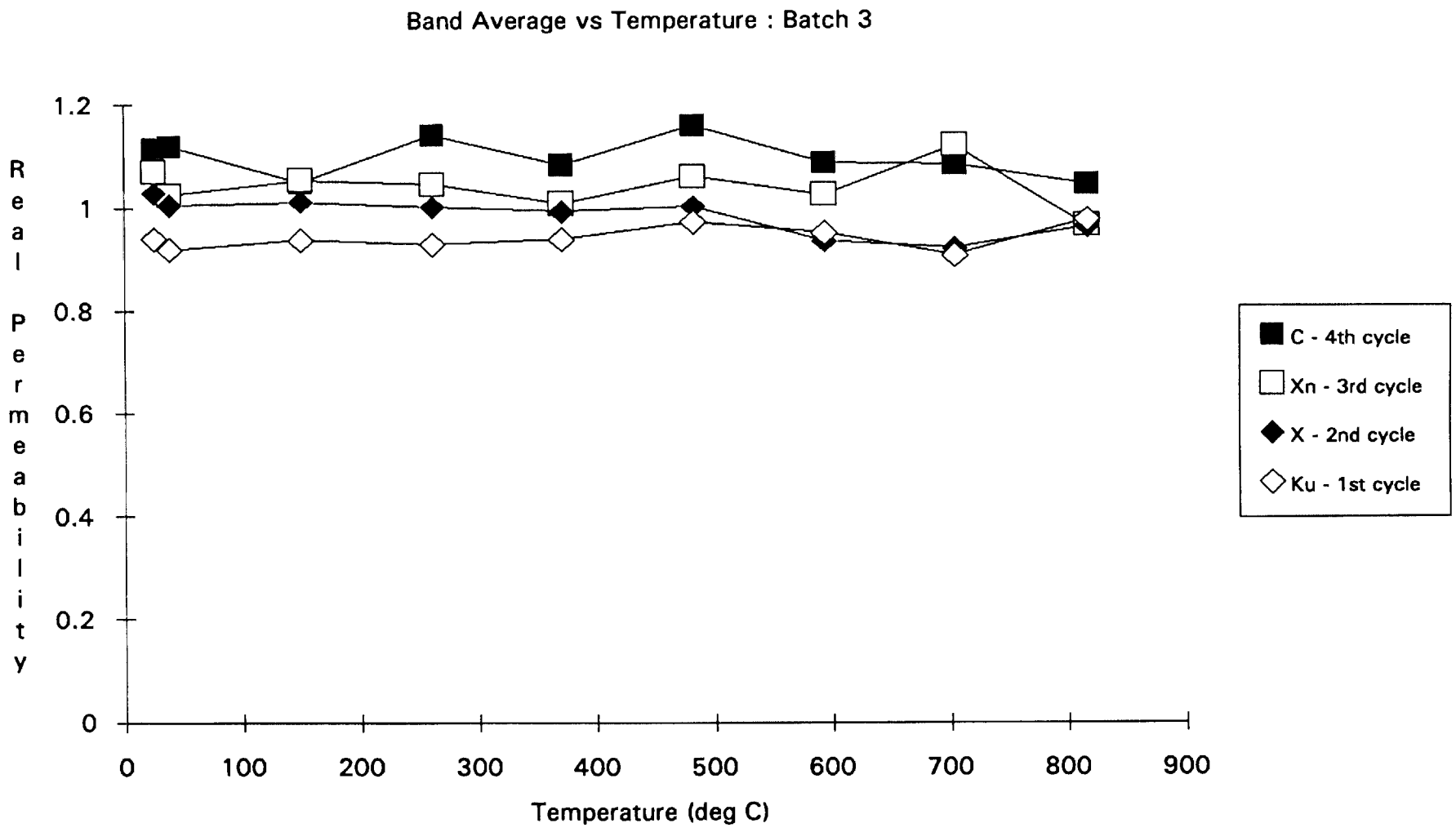

Figure 13. Average measured values for the real permeability of samples in batch 3 through each of four heating cycles. Note all four bands converge to a value near 1 as the temperature approaches 800°C.

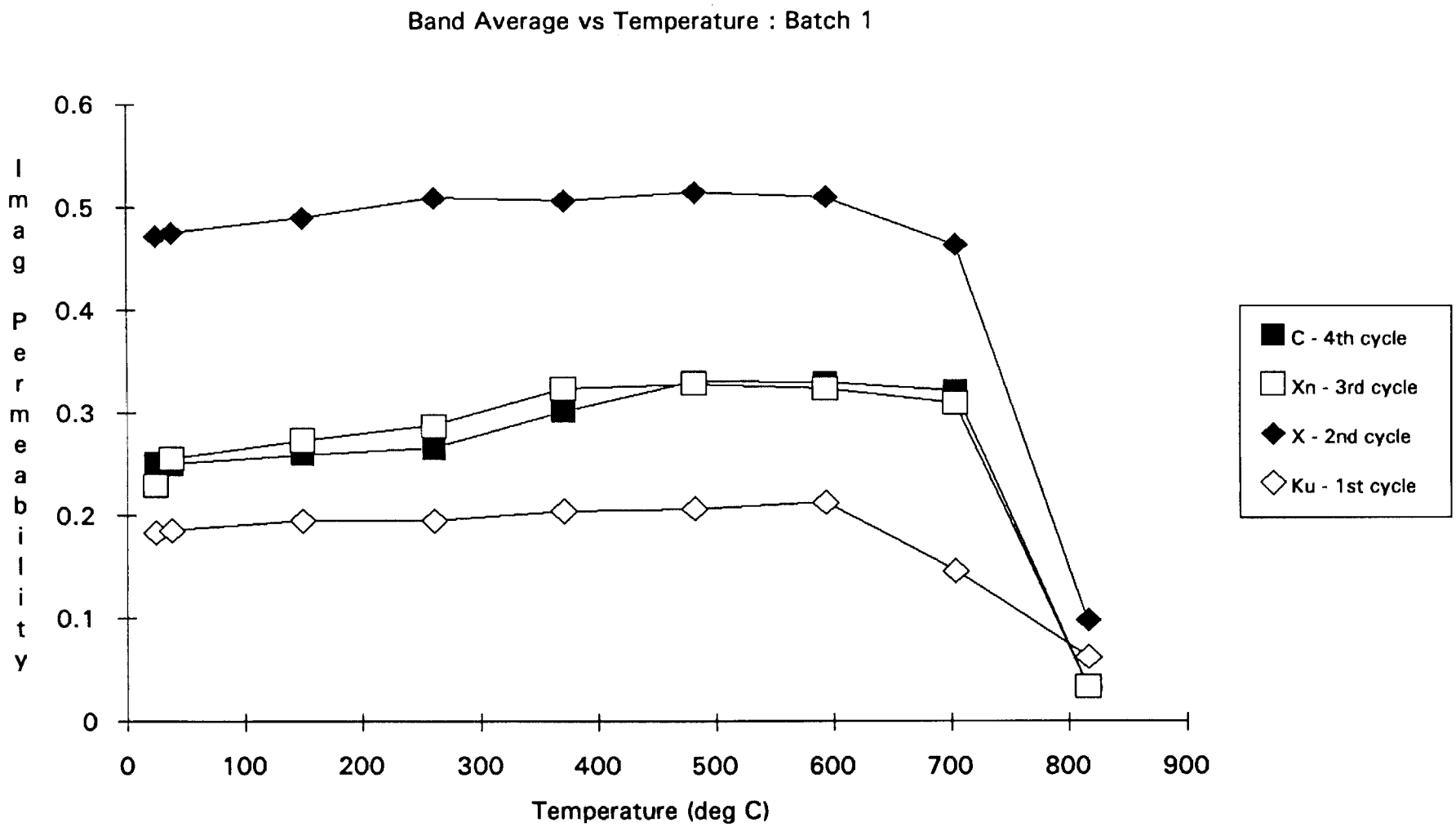

Figure 14. Average measured values for the imaginary permeability of samples in batch 1 through each of four heating cycles. The values reach a maximum in X band. Note that the Curie temperature evidently occurs between 704 and 816°C.

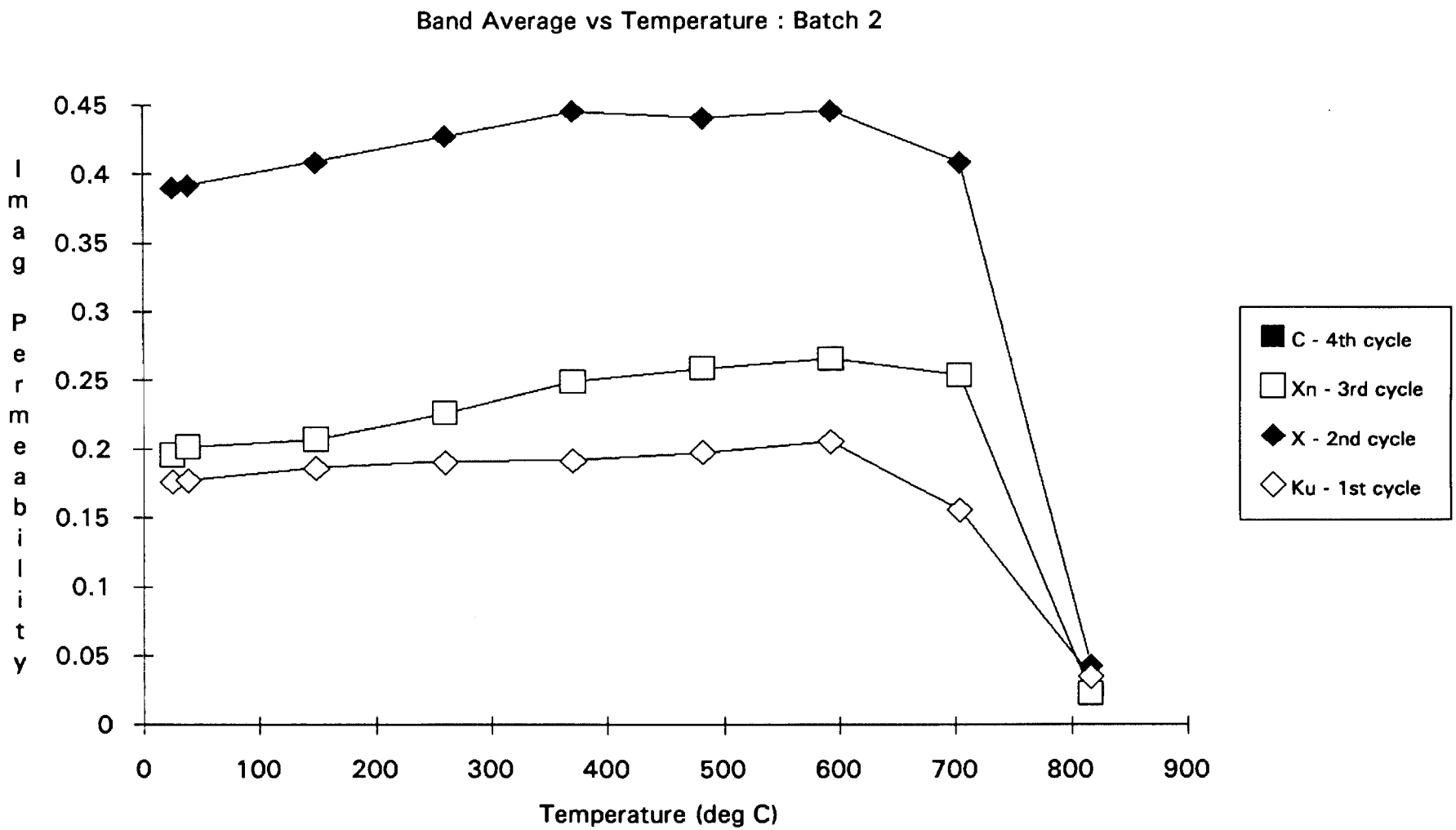

Figure 15. Average measured values for the imaginary permeability of samples in batch 2 through each of four heating cycles. The values reach a maximum in X band. Note that the Curie temperature evidently occurs between 704 and 816°C.

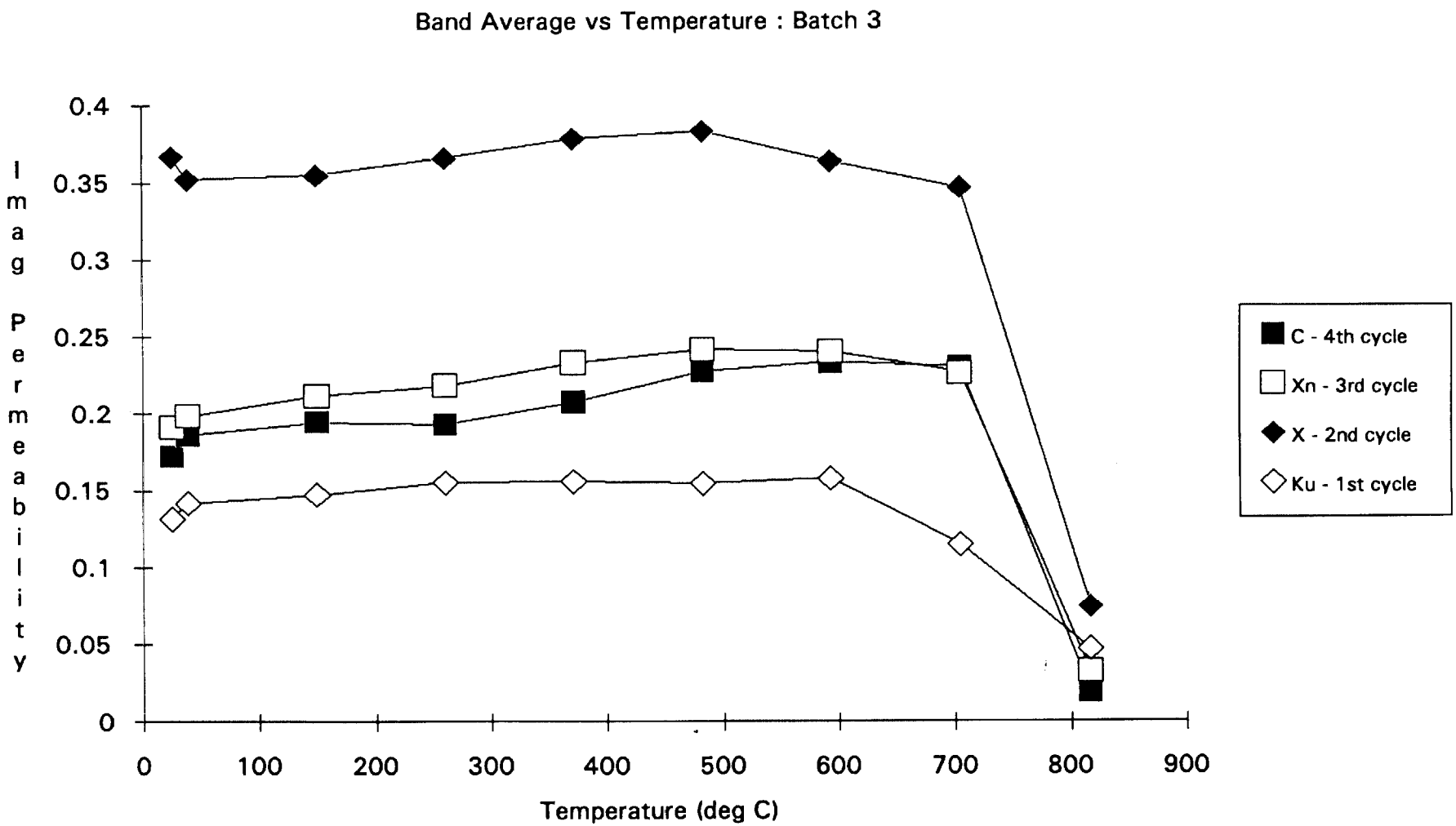

Figure 16. Average measured values for the imaginary permeability of samples in batch 3 through each of four heating cycles. The values reach a maximum in X band. Note that the Curie temperature evidently occurs between 704 and 816°C.

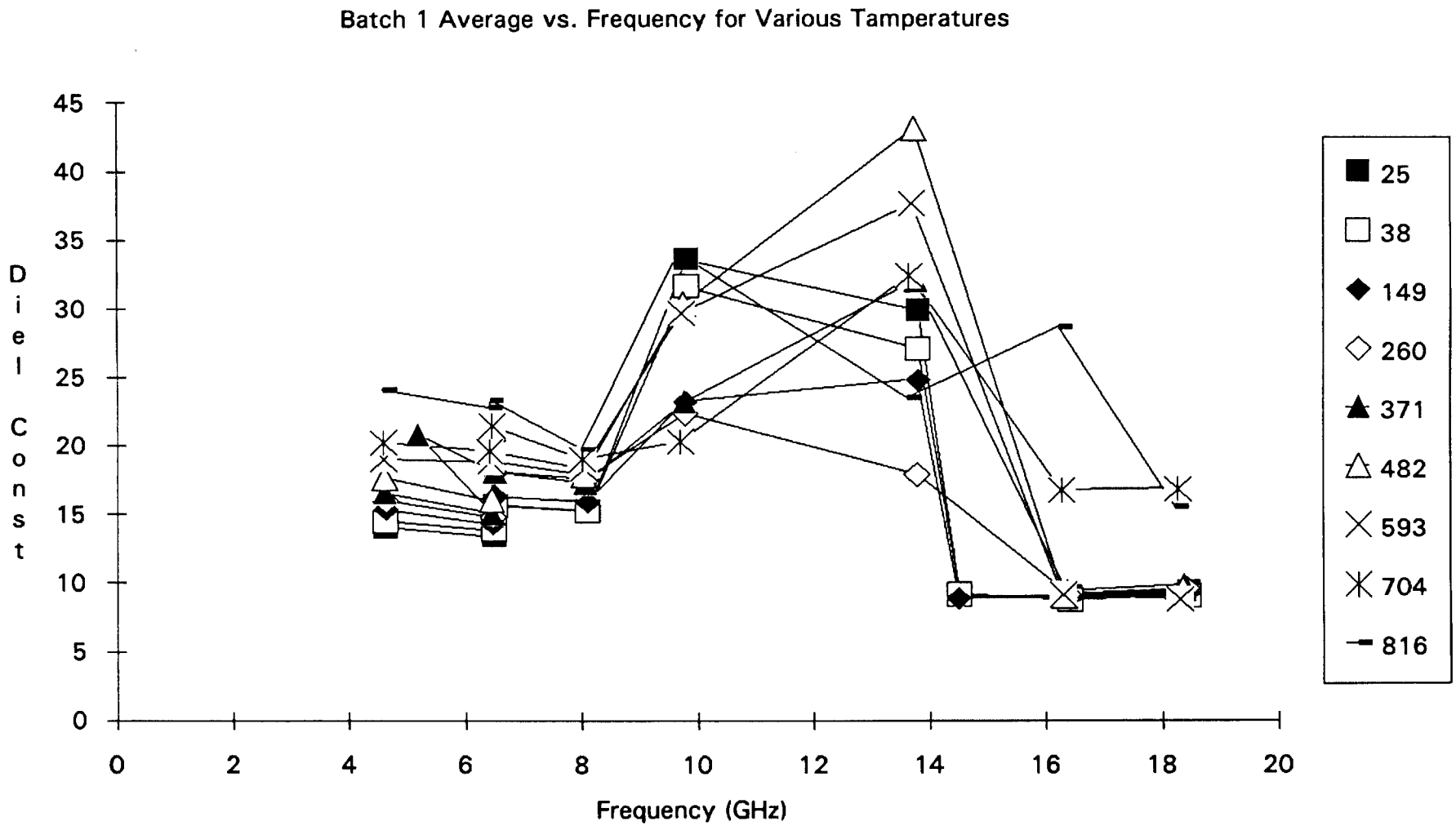

Figure 17. Average measured values for the dielectric constant of samples in batch 1 at each temperature as a function of frequency. Values in Ku and X bands were apparently affected by physical changes in the samples due to heating.

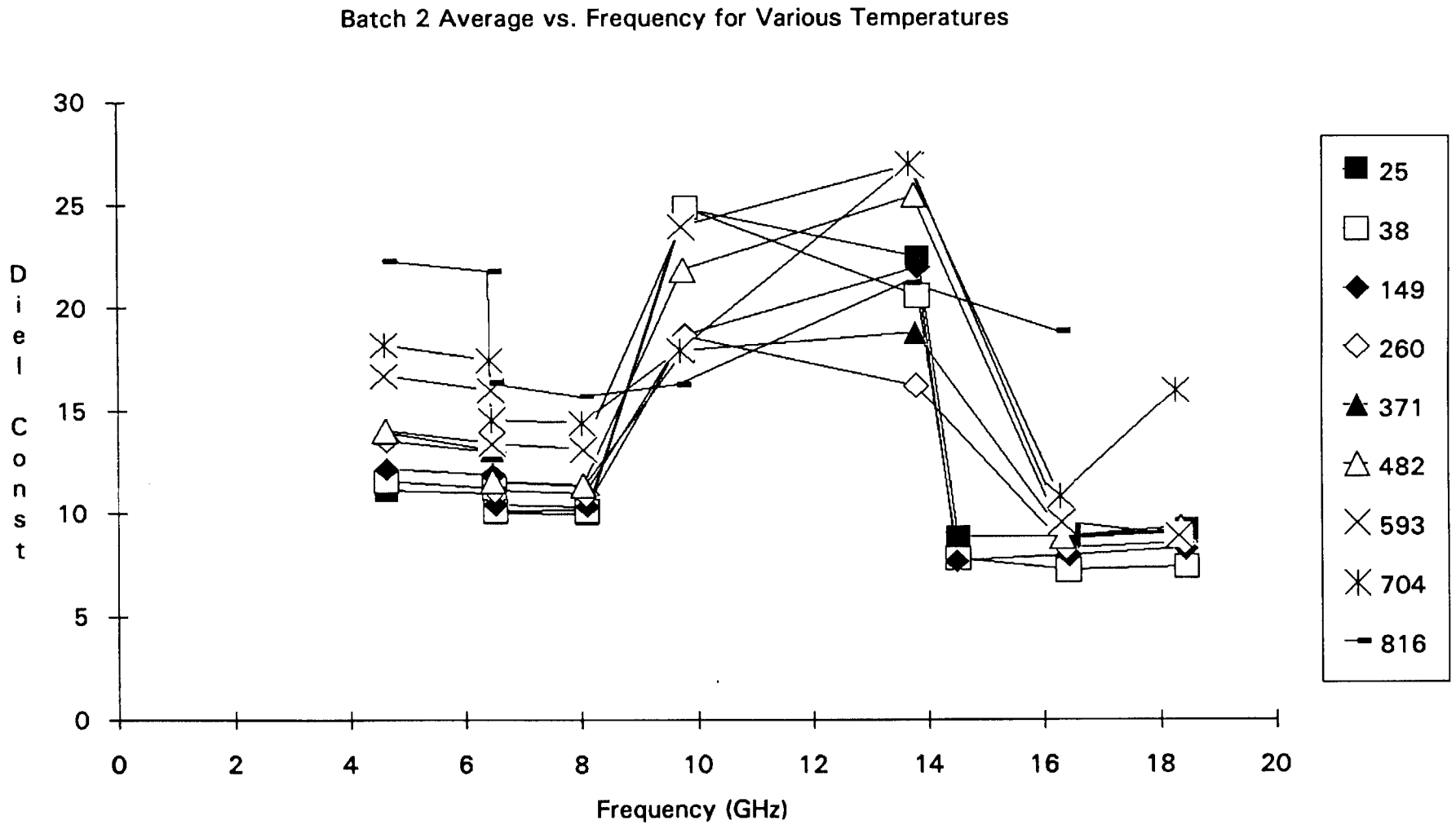

Figure 18. Average measured values for the dielectric constant of samples in batch 2 at each temperature as a function of frequency. Values in Ku and X bands were apparently affected by physical changes in the samples due to heating.

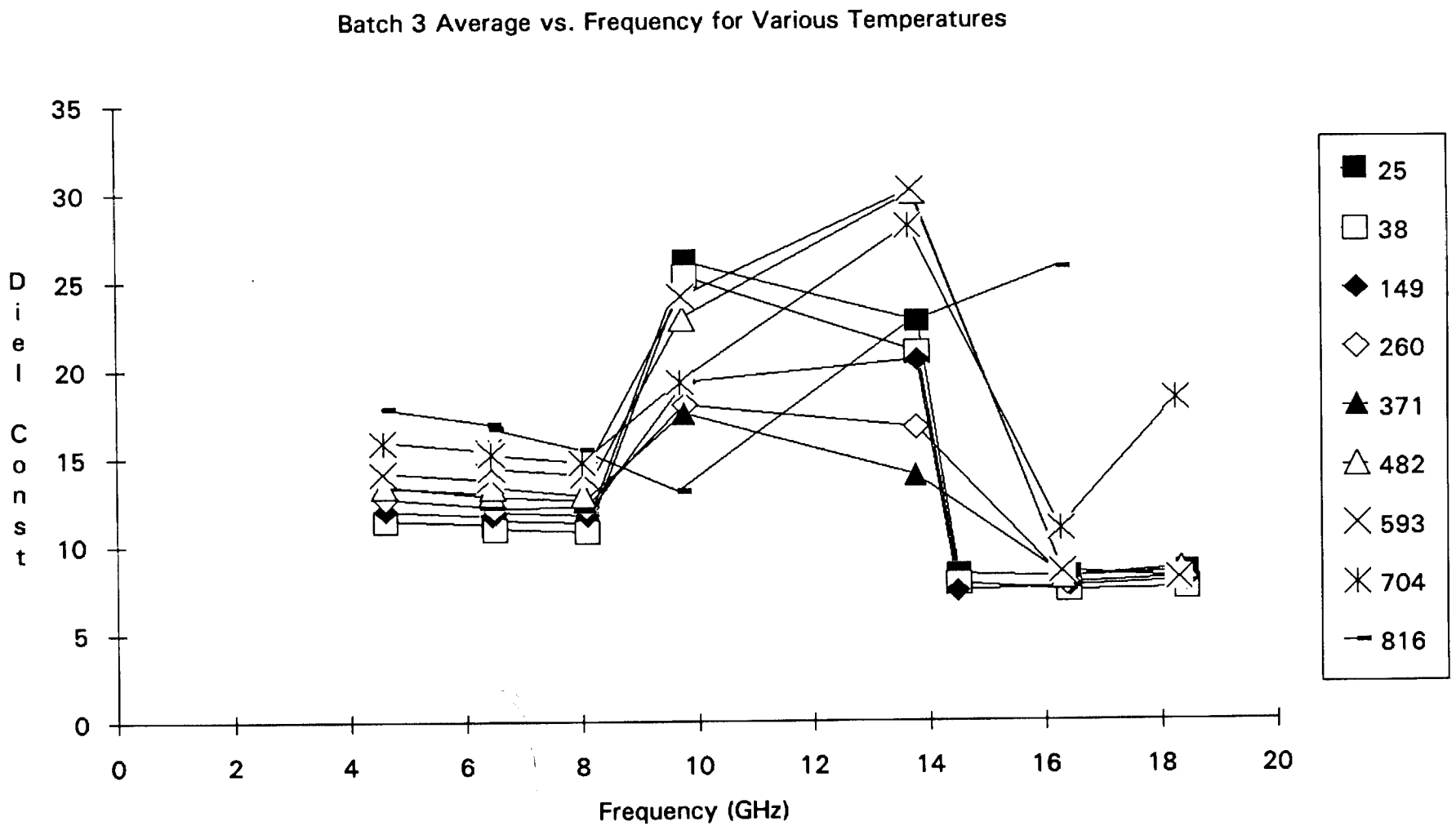

Figure 19. Average measured values for the dielectric constant of samples in batch 3 at each temperature as a function of frequency. Values in Ku and X bands were apparently affected by physical changes in the samples due to heating.

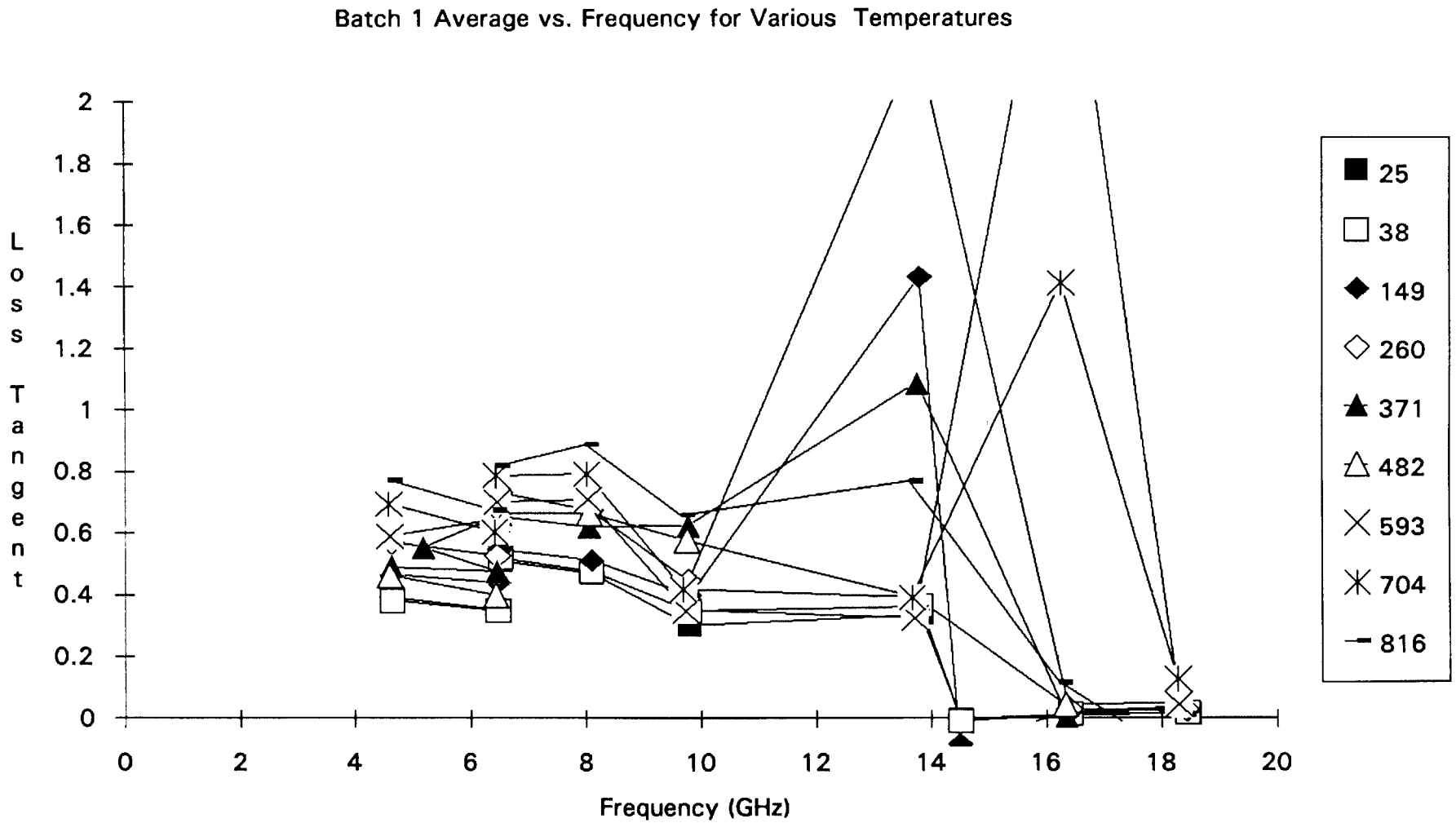

Figure 20. Average measured values for the loss tangent of samples in batch 1 at each temperature as a function of frequency. Values in Ku and X bands were apparently affected by physical changes in the samples due to heating.

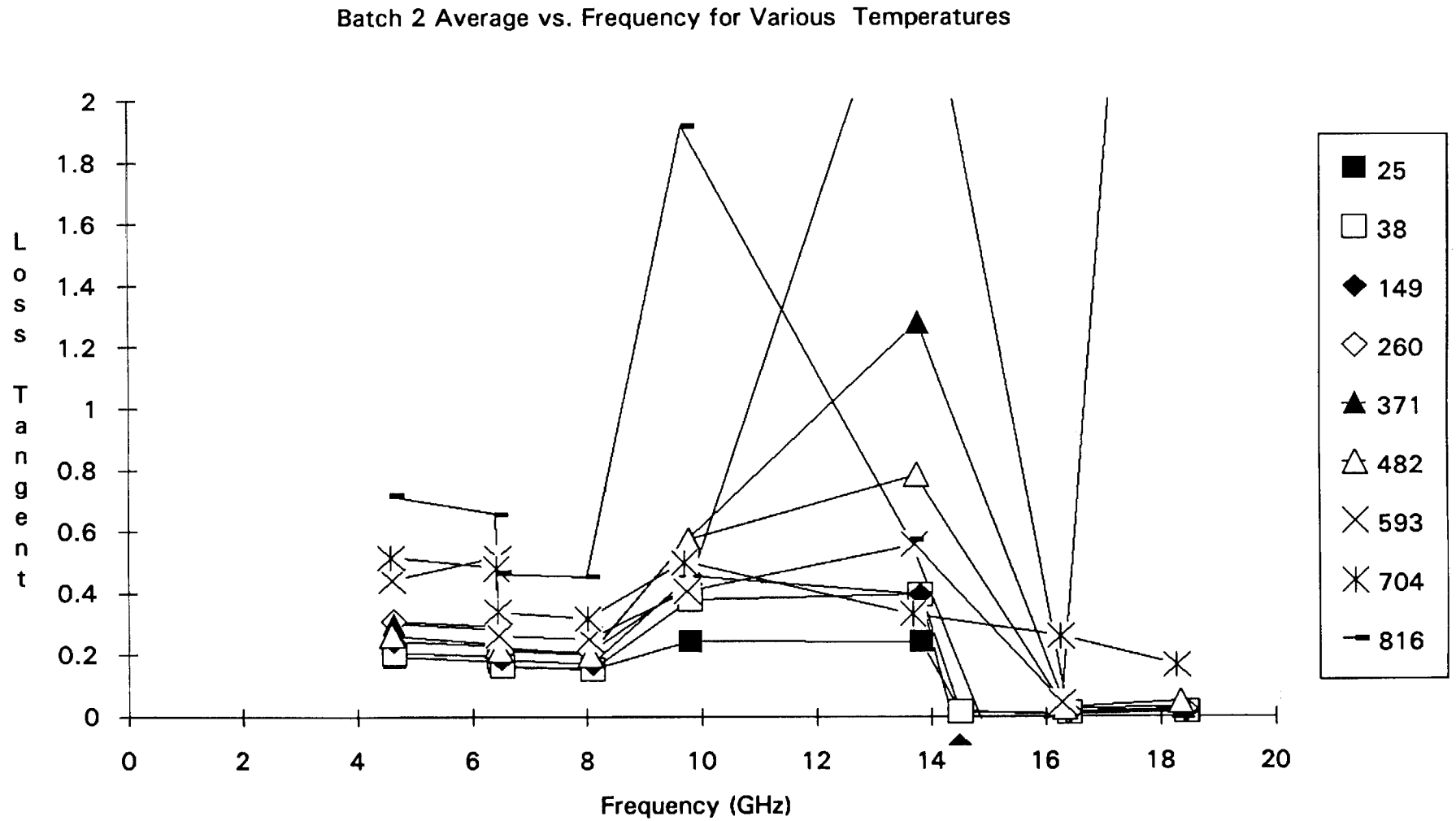

Figure 21. Average measured values for the loss tangent of samples in batch 2 at each temperature as a function of frequency. Values in Ku and X bands were apparently affected by physical changes in the samples due to heating.

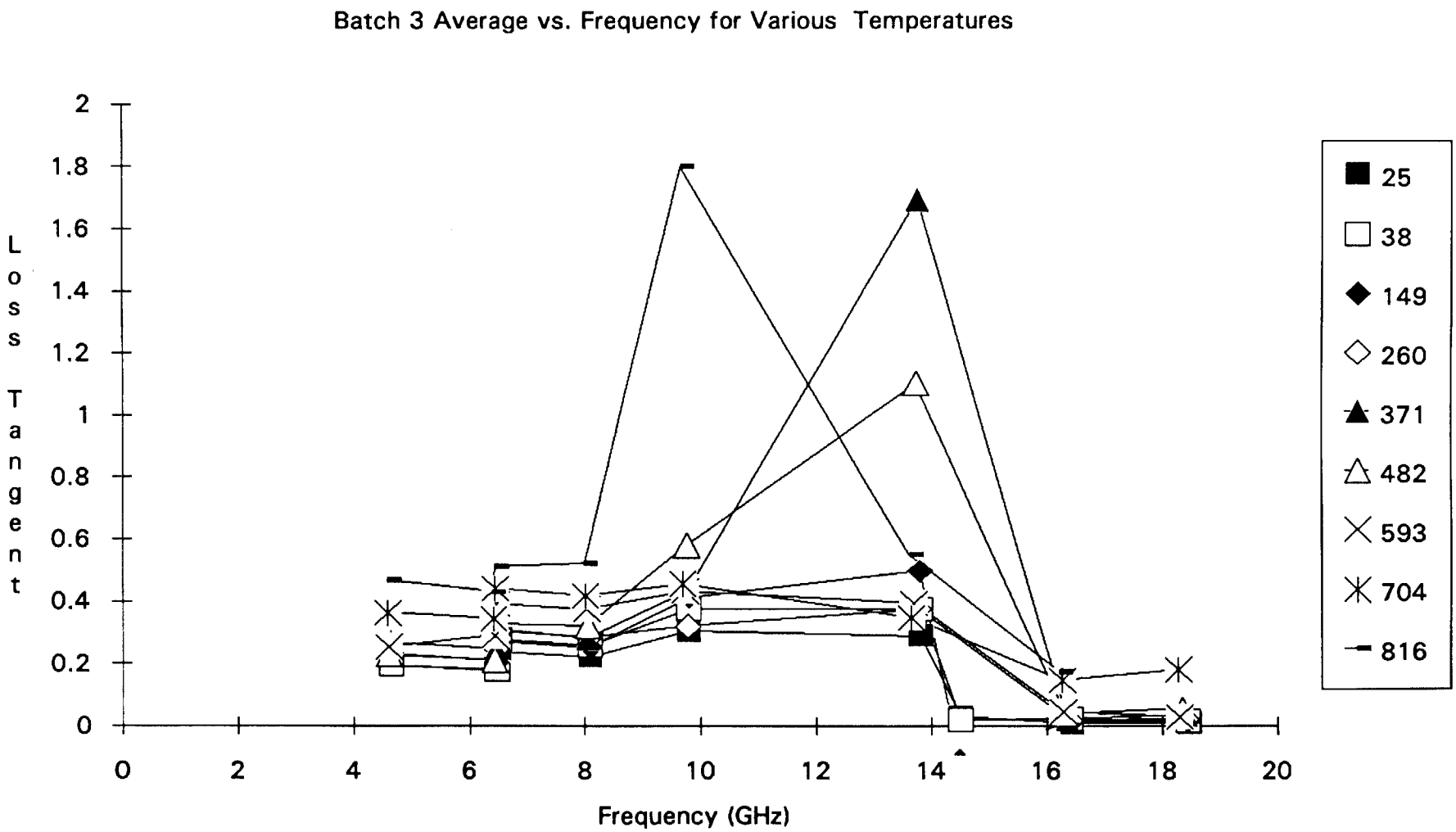

Figure 22. Average measured values for the loss tangent of samples in batch 3 at each temperature as a function of frequency. Values in Ku and X bands were apparently affected by physical changes in the samples due to heating.

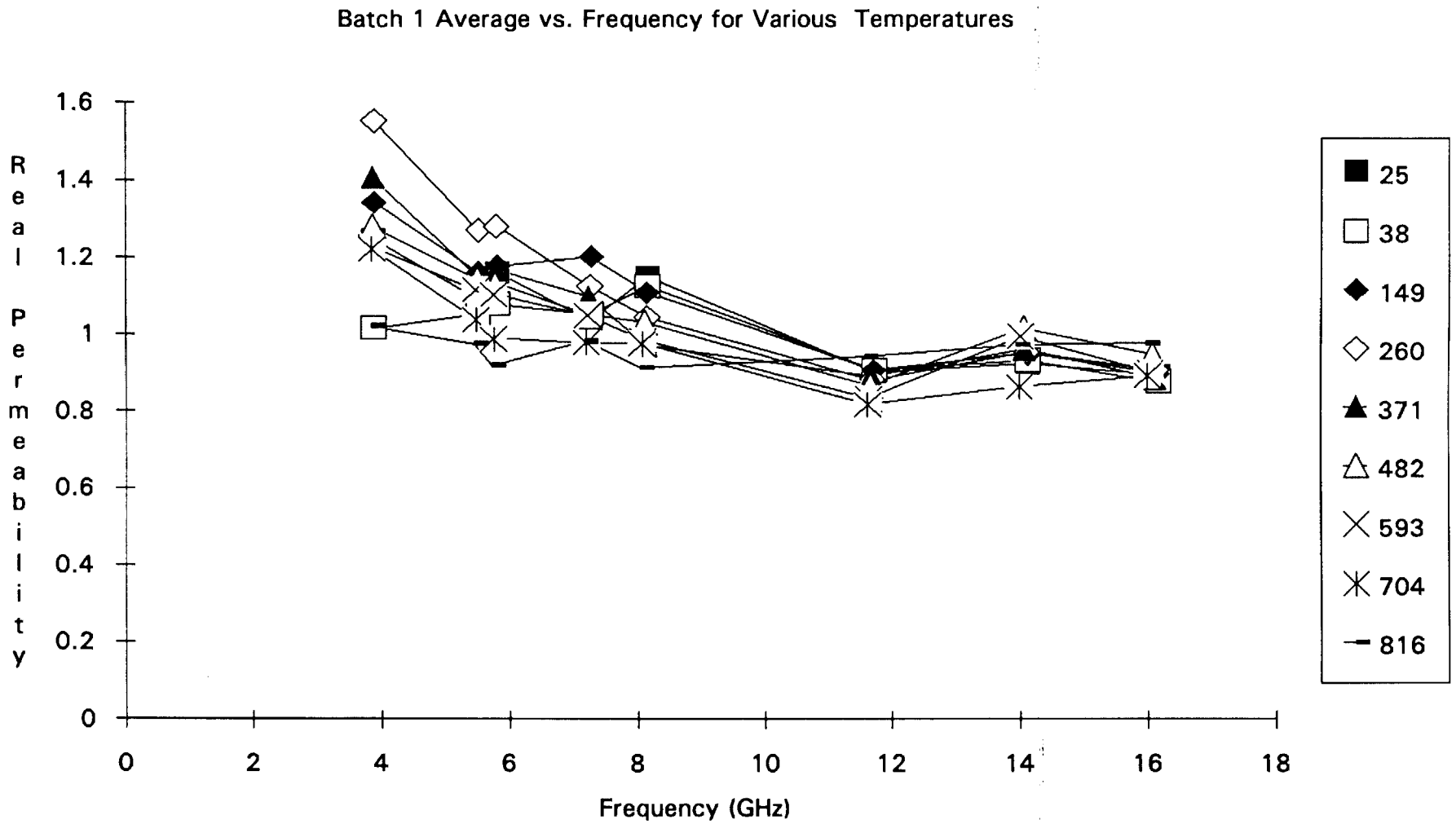

Figure 23. Average measured values for the real permeability of samples in batch 1 at each temperature as a function of frequency.

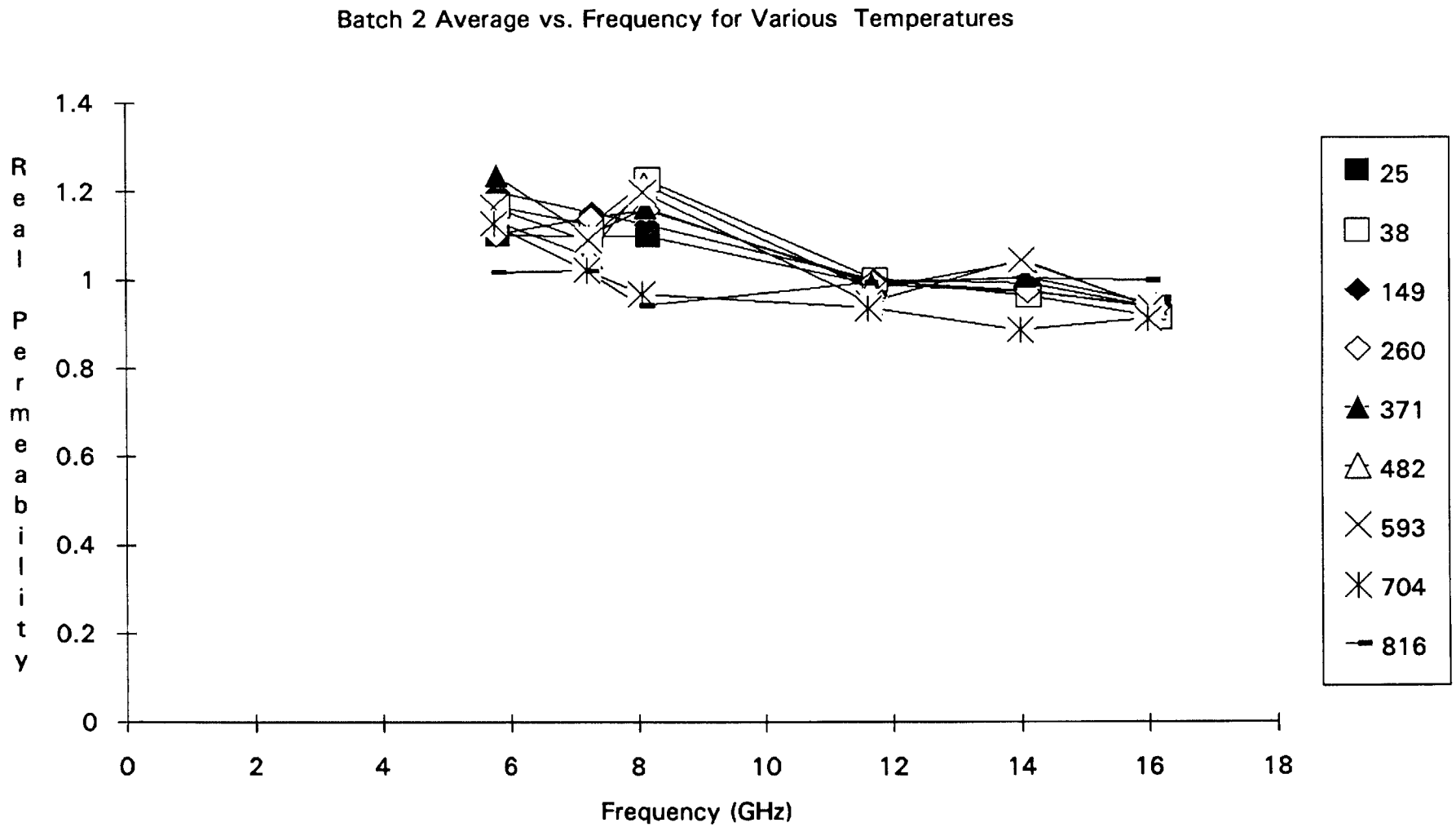

Figure 24. Average measured values for the real permeability of samples in batch 2 at each temperature as a function of frequency.

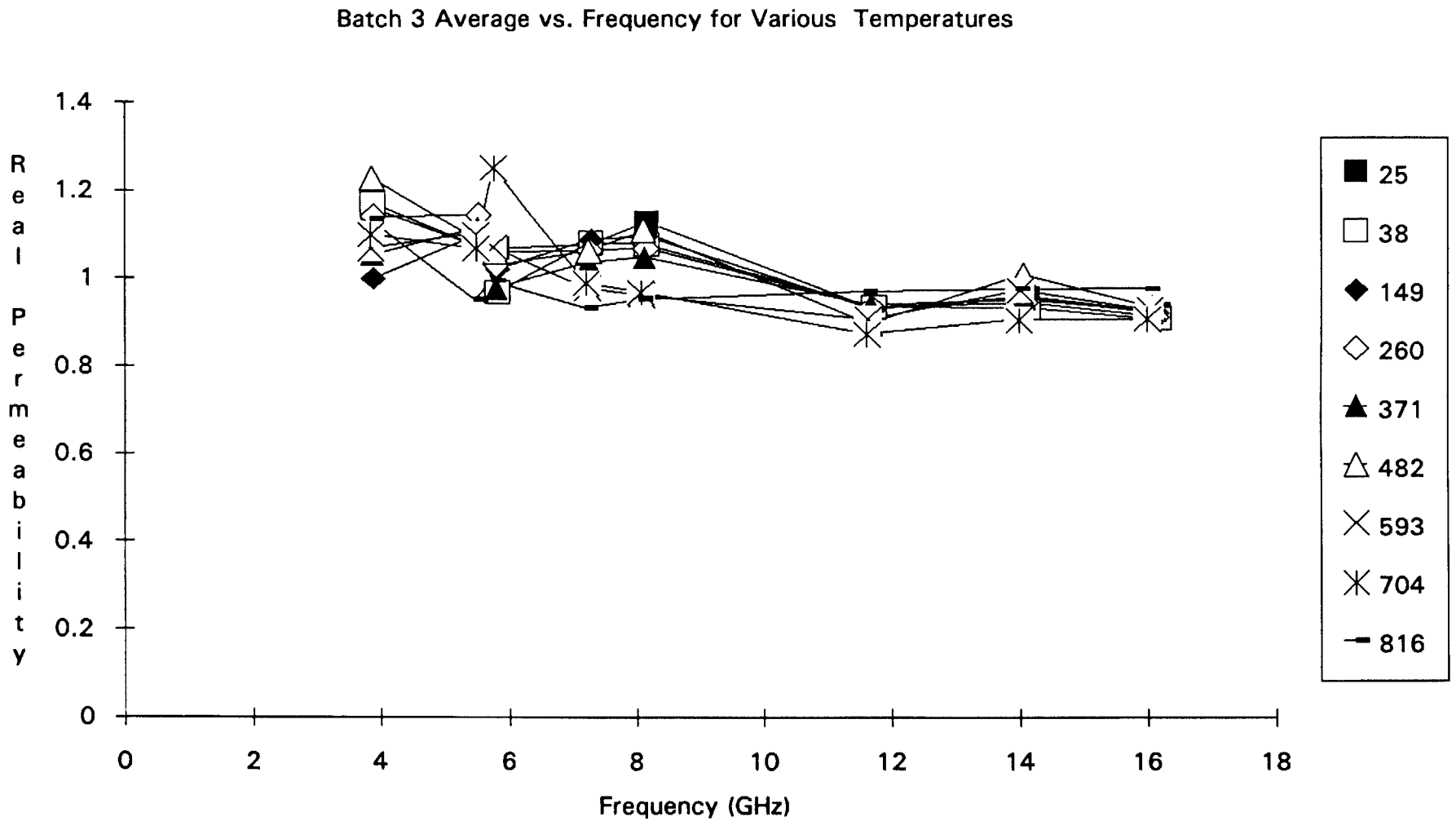

Figure 25. Average measured values for the real permeability of samples in batch 3 at each temperature as a function of frequency.

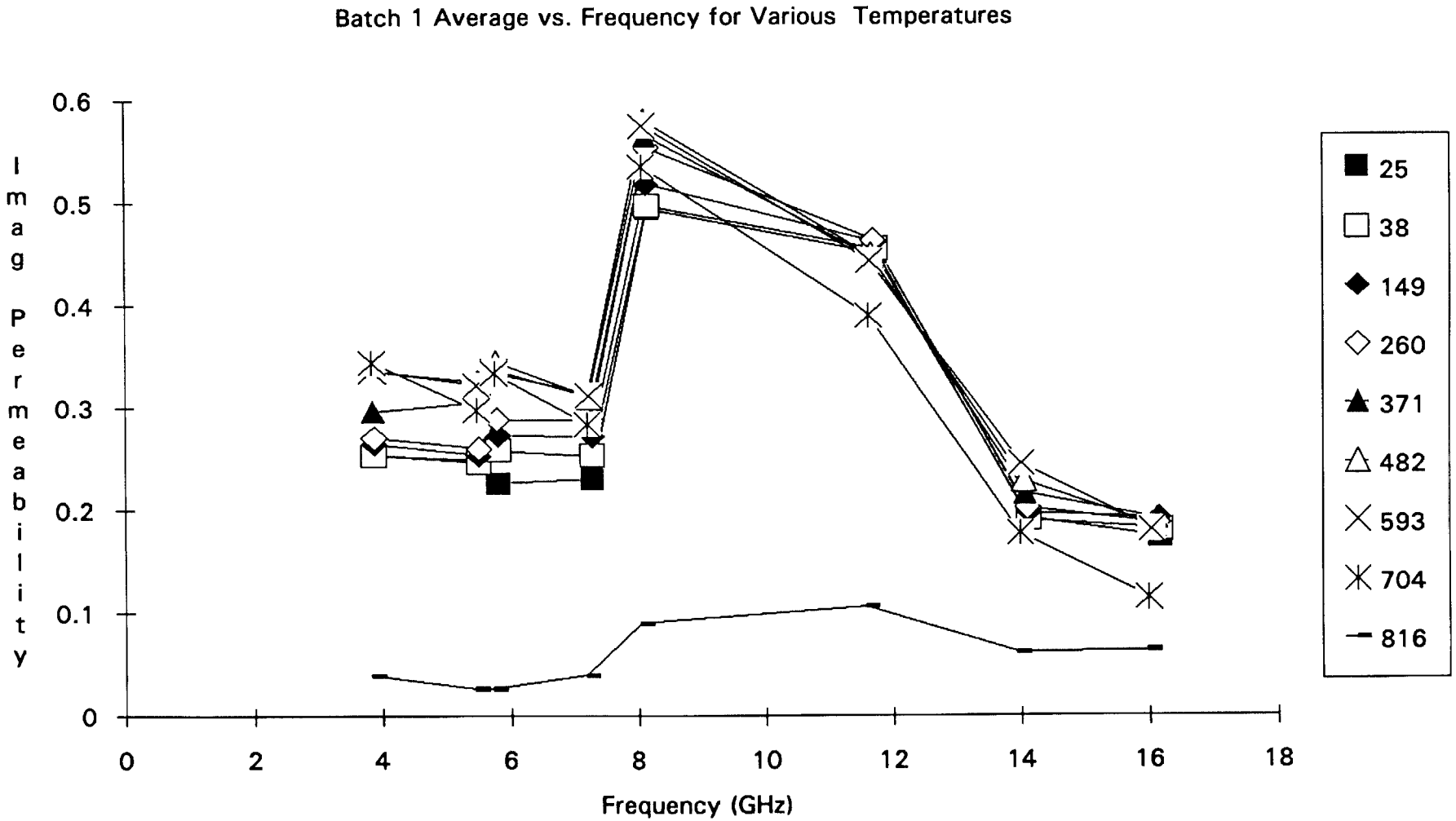

Figure 26. Average measured values for the imaginary permeability of samples in batch 1 at each temperature as a function of frequency. Note values are approaching zero at the highest temperature (816°C).

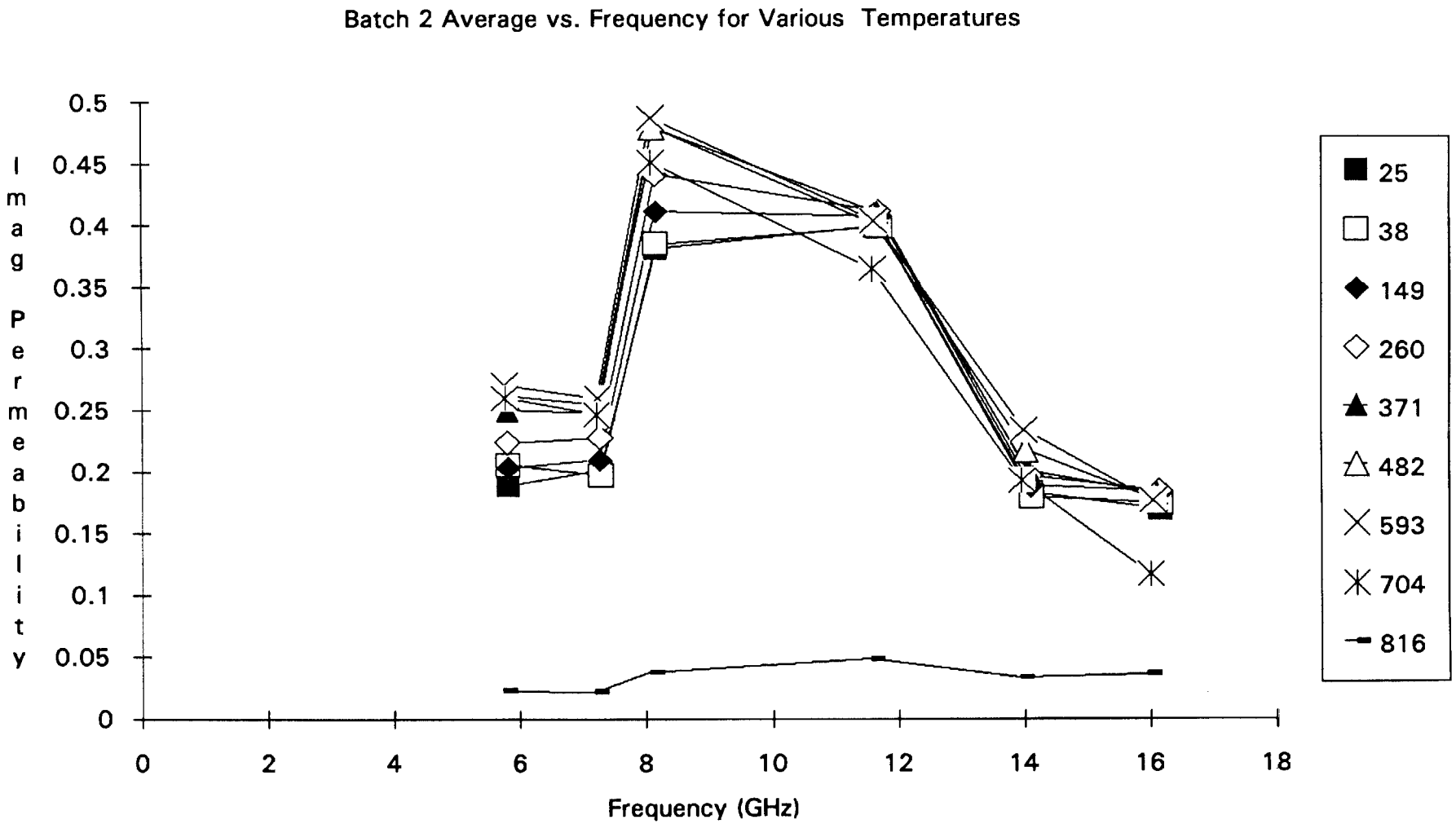

Figure 27. Average measured values for the imaginary permeability of samples in batch 2 at each temperature as a function of frequency. Note values are approaching zero at the highest temperature (816°C).

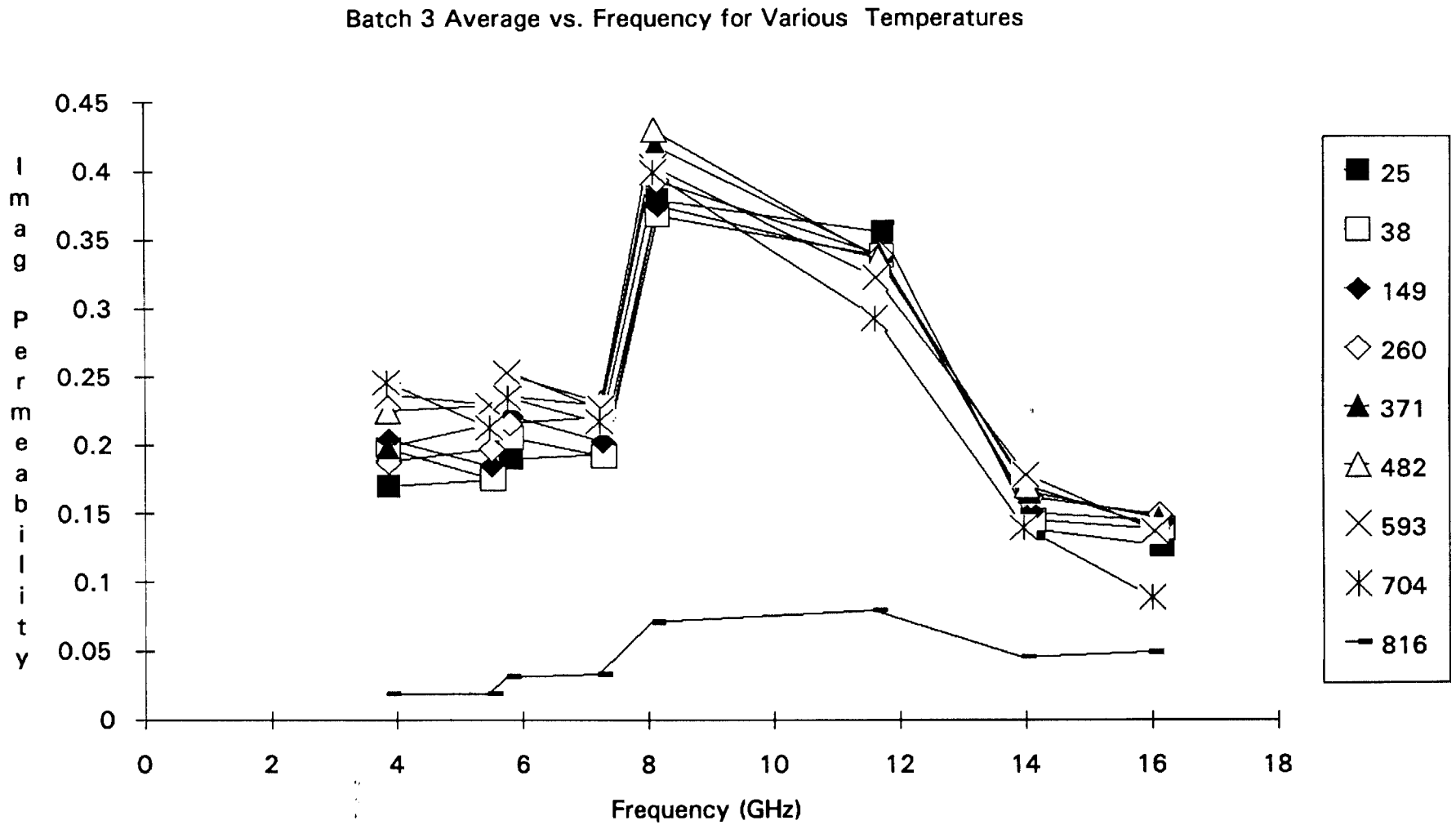

Figure 28. Average measured values for the imaginary permeability of samples in batch 3 at each temperature as a function of frequency. Note values are approaching zero at the highest temperature (816°C).

E. Error Analysis

The data points in Figures 5-16 are plotted again in Figures 29-40 with error bars. This section will present the analysis by which the error bars were obtained. The equations by which the real and imaginary parts of the permittivity are calculated simplify essentially to the following:

$$\varepsilon_r - 1 = \frac{f_0 - f_s}{f_0} \cdot \frac{V_c}{2V_s} = \frac{F_r \cdot V_r}{2}$$

$$\varepsilon_i = \left(\frac{1}{Q_s} - \frac{1}{Q_0}\right) \cdot \frac{V_c}{4V_s} = \Delta\left(\frac{1}{Q}\right) \cdot \frac{V_r}{4}$$

Where

$$F_r = \frac{f_0 - f_s}{f_0}$$

$$V_r = \frac{V_c}{V_s}$$

$$\Delta\left(\frac{1}{Q}\right) = \left(\frac{1}{Q_s} - \frac{1}{Q_0}\right)$$

The real and imaginary parts of the permittivity are, of course, represented by ε_r and ε_i, respectively. The other variables are:

V_C	Volume of the cavity
V_S	Volume of sample inside the cavity
f_0	Resonant frequency of the empty cavity
f_S	Resonant frequency with the sample present

Q_0 Quality factor of the empty cavity

Q_S Quality factor with the sample present

The uncertainties in these quantities are related by

$$2\,\sigma^2(\varepsilon_r) = \sigma^2(F_r)\cdot\left(\frac{\partial\varepsilon_r}{\partial F_r}\right)^2 + \sigma^2(V_r)\cdot\left(\frac{\partial\varepsilon_r}{\partial V_r}\right)^2$$

$$\sigma^2(\varepsilon_r) = \frac{1}{2}\left(\sigma^2(F_r)\cdot V_r^2 + \sigma^2(V_r)\cdot F_r^2\right)$$

and

$$4\,\sigma^2(\varepsilon_i) = \sigma^2\left(\Delta\left(\frac{1}{Q}\right)\right)\cdot\left|\frac{\partial\varepsilon_i}{\partial\Delta\left(\frac{1}{Q}\right)}\right|^2 + \sigma^2(V_r)\cdot\left(\frac{\partial\varepsilon_i}{\partial V_r}\right)^2$$

$$\sigma^2(\varepsilon_i) = \frac{1}{4}\left(\sigma^2\left(\Delta\left(\frac{1}{Q}\right)\right)\cdot V_r^2 + \sigma^2(V_r)\cdot\Delta\left(\frac{1}{Q}\right)^2\right)$$

where the standard deviation in a sample population is taken as the uncertainty. It is also necessary that the measurement uncertainty in the volume term be independent of the measurement uncertainty in the frequency term or quality factor term. Then the uncertainty in these terms can be determined from physical measurement considerations.

For the volume ratio term, the uncertainty is derived from

$$\sigma^2(V_r) = \sigma^2(V_c) \cdot \left(\frac{\partial V_r}{\partial V_c}\right)^2 + \sigma^2(V_s) \cdot \left(\frac{\partial V_r}{\partial V_s}\right)^2$$

$$= \left[\sigma^2(V_s) \cdot \left(\frac{V_c}{V_s}\right)^2 + \sigma^2(V_c)\right] \Big/ V_s^2$$

The cavity volume contributes

$$\sigma^2(V_c) = \sigma^2(a)(b\ell)^2 + \sigma^2(b)(a\ell)^2 + \sigma^2(\ell)(ab)^2$$

where the uncertainty in the transverse dimensions, a and b, are the mechanical tolerances of the waveguide, and the measurement uncertainty of 0.08 cm (0.03 in.) in the length is used for $\sigma(\ell)$.

The volume of sample in the cavity is calculated for each measurement using the appropriate transverse waveguide dimension (broad wall for permeability measurements and narrow wall for permittivity measurements) and the cross sectional area of the individual sample. The sample cross section is assumed to be uniform and is calculated using the density values supplied with the samples after weighing each sample and measuring its length. Then the sample volume uncertainty is

$$\sigma^2(V_s) = \sigma^2(x)(\ell_s)^2 + \sigma^2(\ell_s)(x)^2$$

where ℓ_s is the length of sample in the cavity and x is the cross section area. Of particular concern is the effect of the value used for the density of a sample material. The precision of the density value supplied with the samples was taken to be $\pm$.01 g/cc. With this precision for the density, and assuming a uniform sample cross-section, the uncertainty in the sample volume is dominated by the uncertainty in the measured length of the sample, which was determined to be .08 cm (.03 in).

The frequency ratio term F_r contributes to the measurement uncertainty as follows:

$$\sigma^2(F_r) = \sigma^2(f_0)\cdot\left(\frac{\partial F_r}{\partial f_0}\right)^2 + \sigma^2(f_s)\cdot\left(\frac{\partial F_r}{\partial f_s}\right)^2$$

$$= \sigma^2(f_0)\cdot\left(\frac{f_s}{f_0^2}\right)^2 + \sigma^2(f_s)\cdot\left(\frac{1}{f_0^2}\right)$$

Here the variance terms are computed from the measurement results. Specifically, the variance term for the empty cavity resonance, f_0, is calculated as the sample variance for the population of empty cavity resonant frequency values recorded at each mode with each batch of samples. The variance term for the perturbed resonant frequency, f_S, is likewise calculated from the measurement population at each mode for each batch of samples. Note that this means that sample to sample variation within a batch, as well as inhomogeneity within each sample, will contribute to the measurement uncertainty, and this is reflected in the plotted error bars. Similarly, uncertainty in the quality factor measurements is taken as the measurement variance at each mode for each batch of samples, and contributes to the overall measurement uncertainty through the $\Delta\left(\frac{1}{Q}\right)$ term as follows:

$$\sigma^2\left(\left(\Delta\left(\frac{1}{Q}\right)\right)\right) = \sigma^2\left(\frac{1}{Q_s}\right)\cdot\left|\frac{\partial\left(\Delta\left(\frac{1}{Q}\right)\right)}{\partial\left(\frac{1}{Q_s}\right)}\right|^2 + \sigma^2\left(\frac{1}{Q_0}\right)\cdot\left|\frac{\partial\left(\Delta\left(\frac{1}{Q}\right)\right)}{\partial\left(\frac{1}{Q_0}\right)}\right|^2$$

$$= \sigma^2\left(\frac{1}{Q_s}\right) + \sigma^2\left(\frac{1}{Q_0}\right)$$

Again, the effects of sample to sample variation within a sample batch, and the effects of inhomogeneity within a particular sample, have been accounted for in the error bars for these terms.

Finally, the error bars on the loss tangent plots are obtained from the error calculations for the imaginary and real parts of the permittivity. Since the loss tangent is simply the ratio of the imaginary part to the real part, the uncertainties are related by

$$\sigma^2(\tan\delta) = \frac{\sigma^2(\varepsilon_i)}{\varepsilon_r{}^2} + \sigma^2(\varepsilon_r) \cdot \left(\frac{\varepsilon_i}{\varepsilon_r{}^2}\right)^2$$

The results of these calculations are plotted in Figures 32-34.

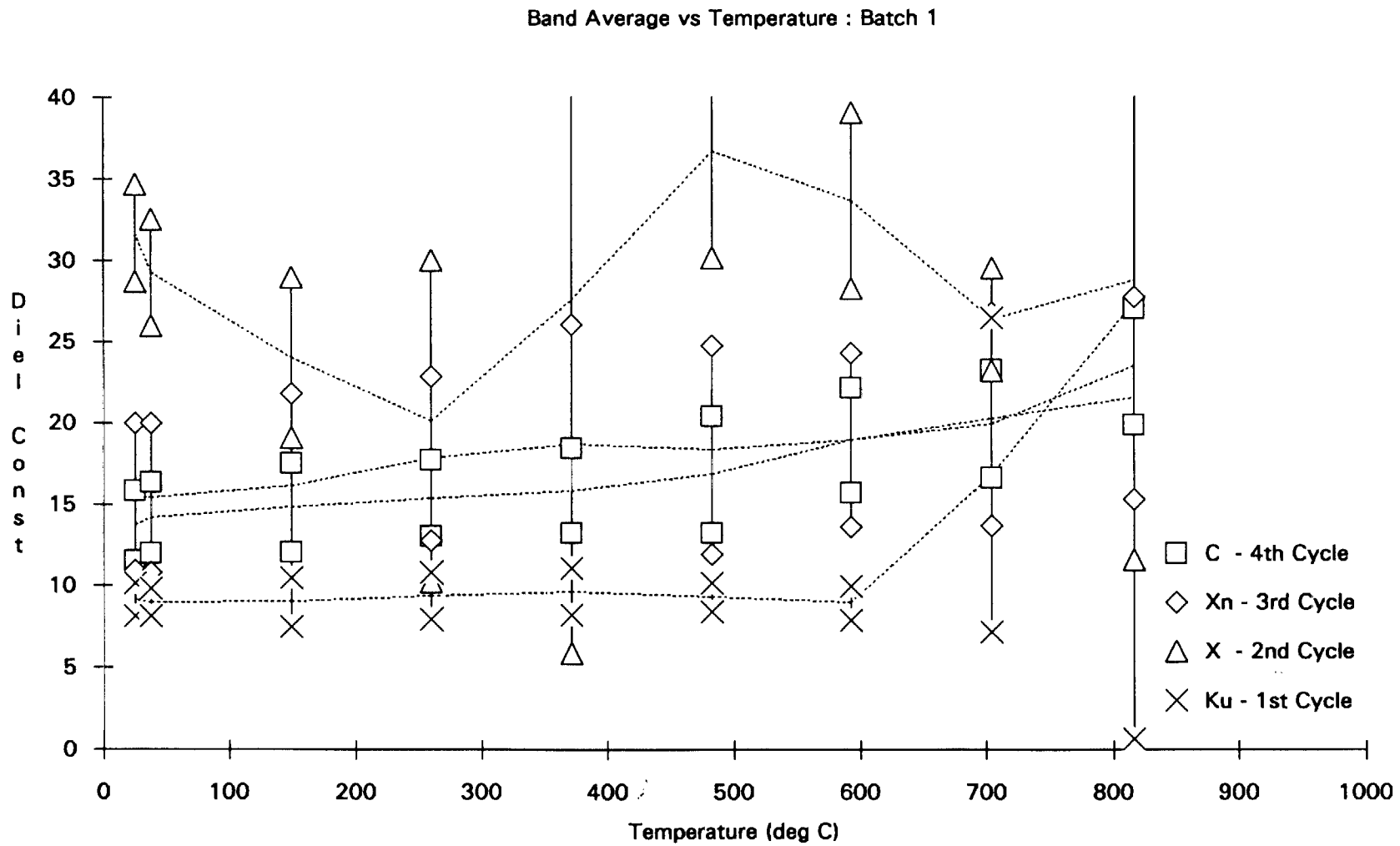

Figure 29. Average measured values with error bars for the dielectric constant of samples in batch 1 through each of four heating cycles. The error bars include variations from sample to sample.

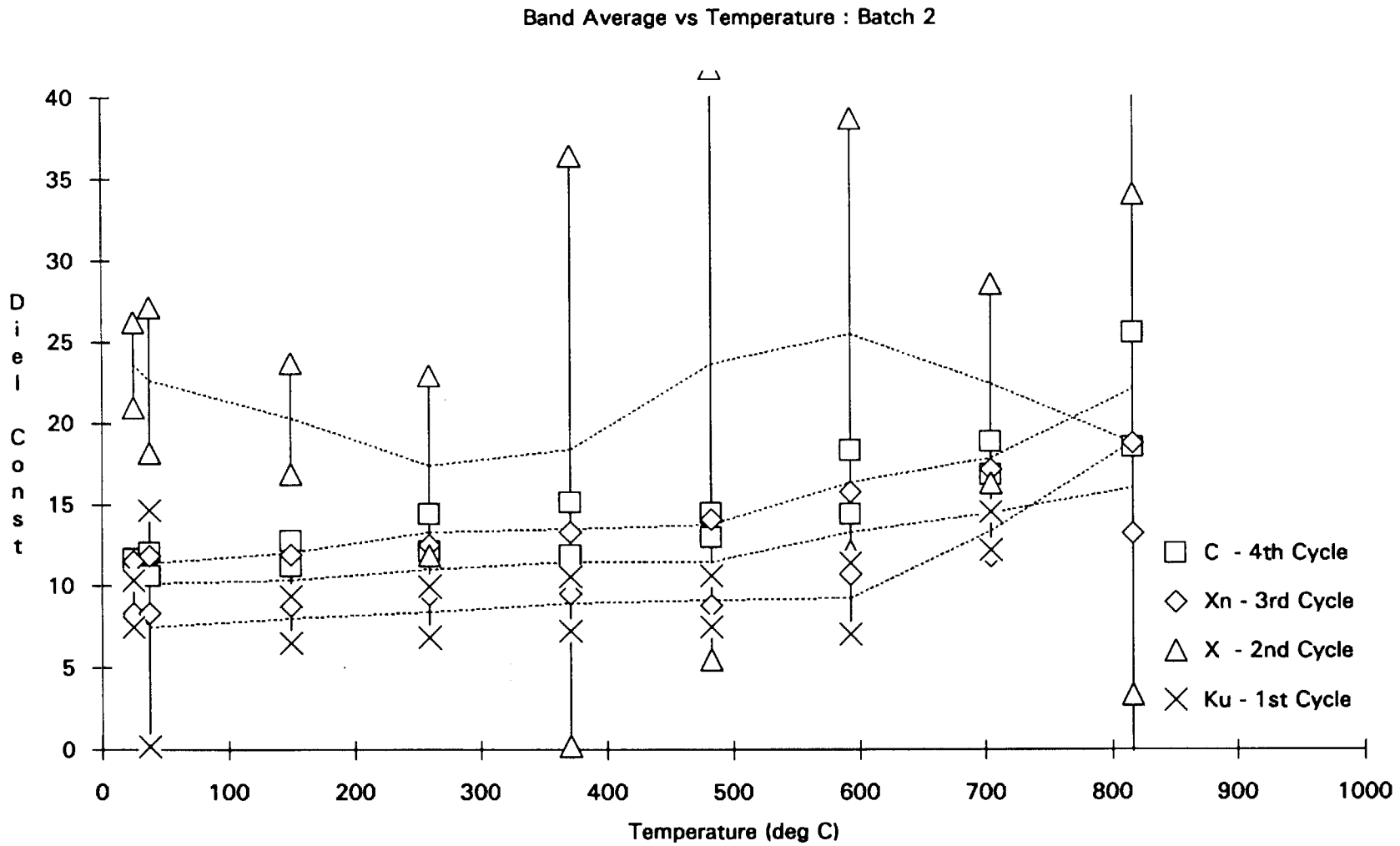

Figure 30. Average measured values with error bars for the dielectric constant of samples in batch 2 through each of four heating cycles. The error bars include variations from sample to sample.

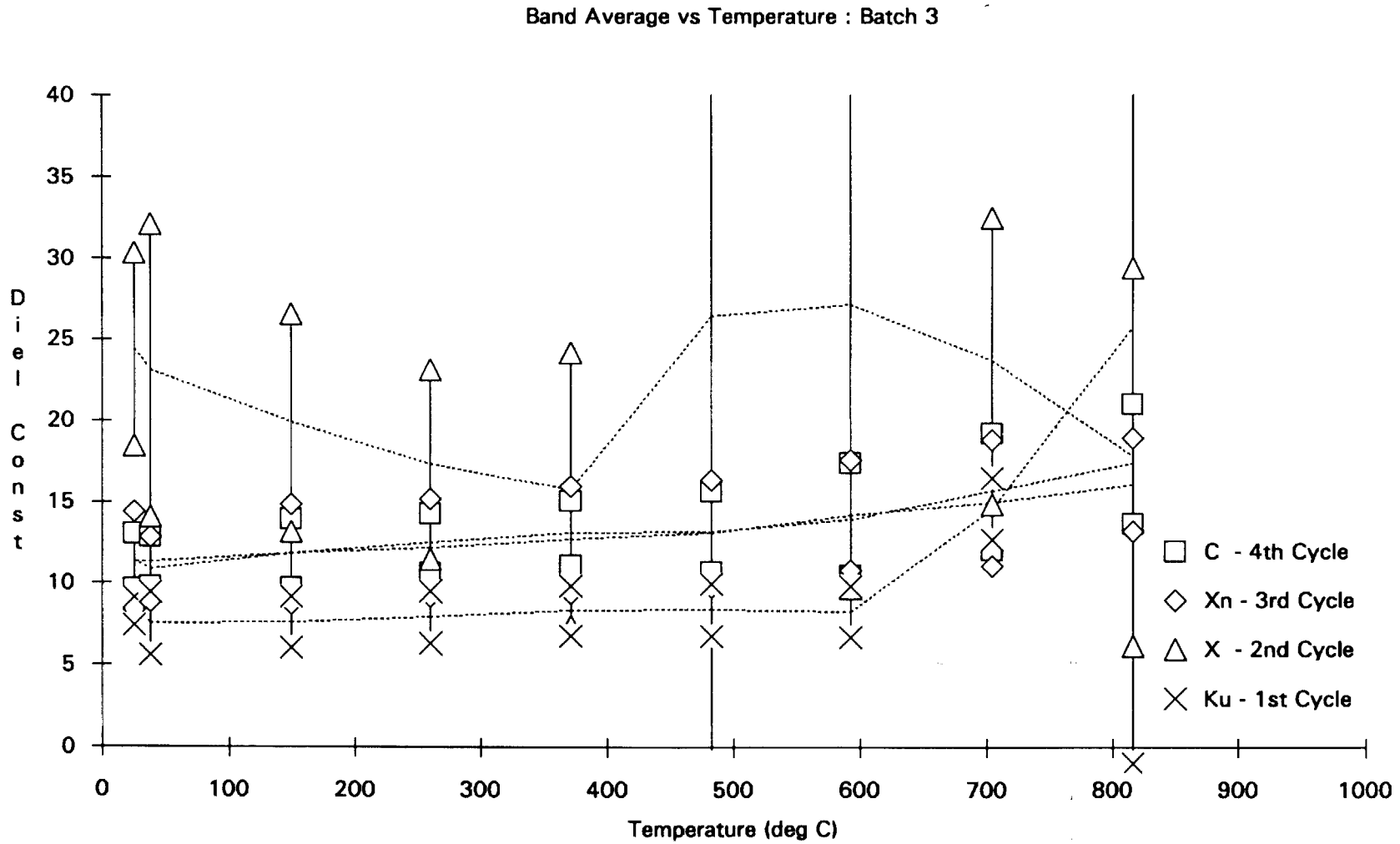

Figure 31. Average measured values with error bars for the dielectric constant of samples in batch 3 through each of four heating cycles. The error bars include variations from sample to sample.

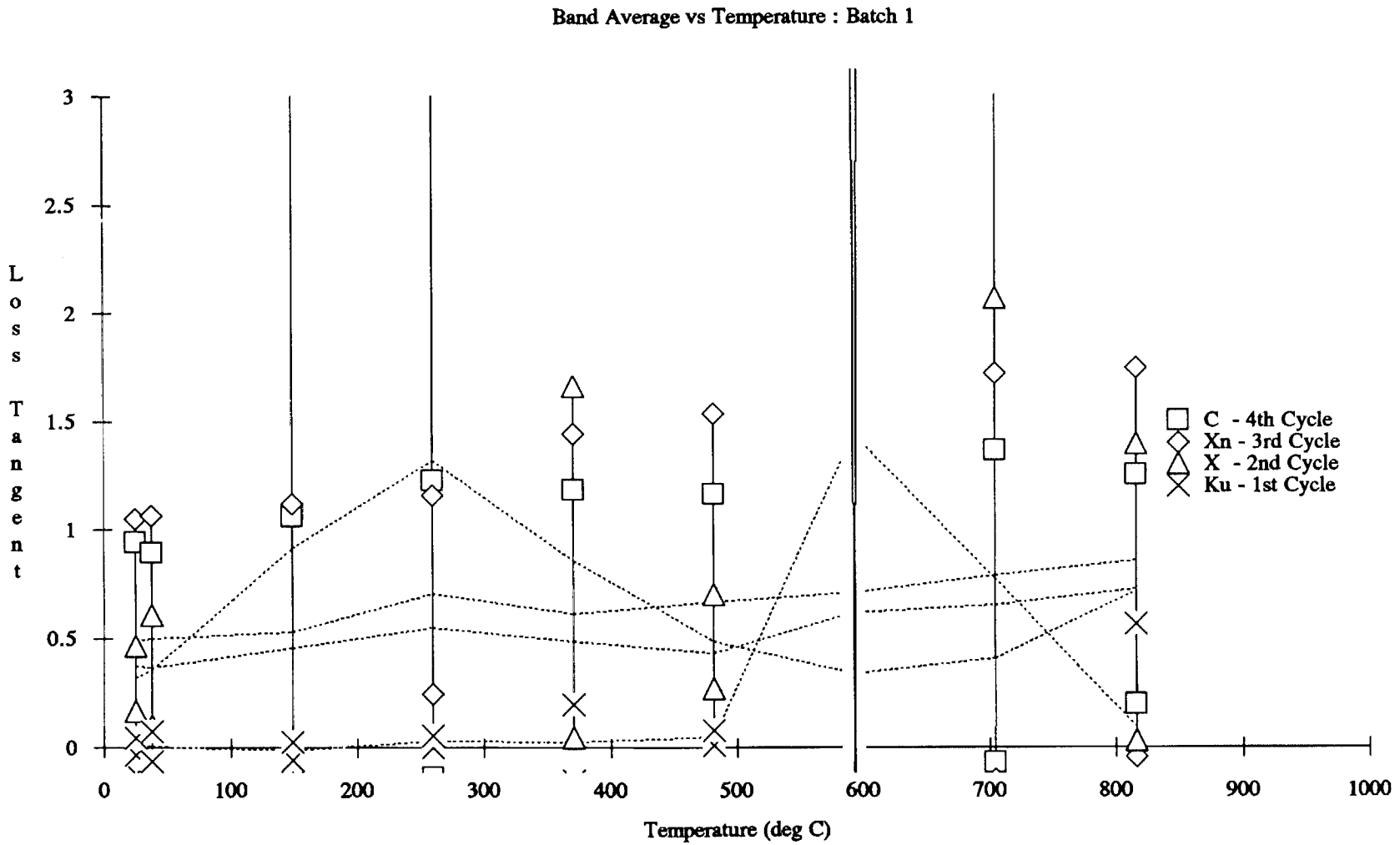

Figure 32. Average measured values with error bars for the loss tangent of samples in batch 1 through each of four heating cycles. The error bars include variations from sample to sample.

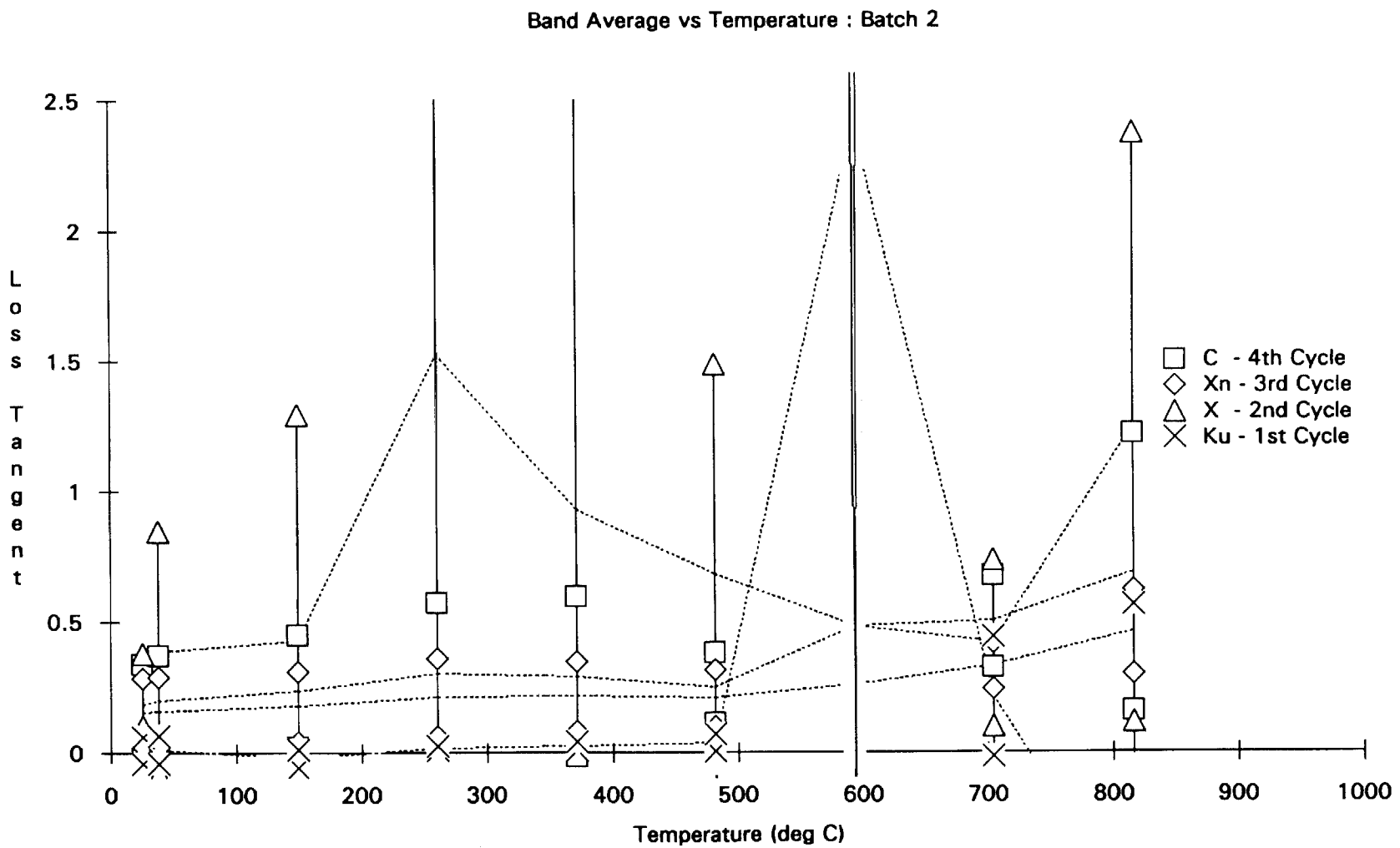

Figure 33. Average measured values with error bars for the loss tangent of samples in batch 2 through each of four heating cycles. The error bars include variations from sample to sample.

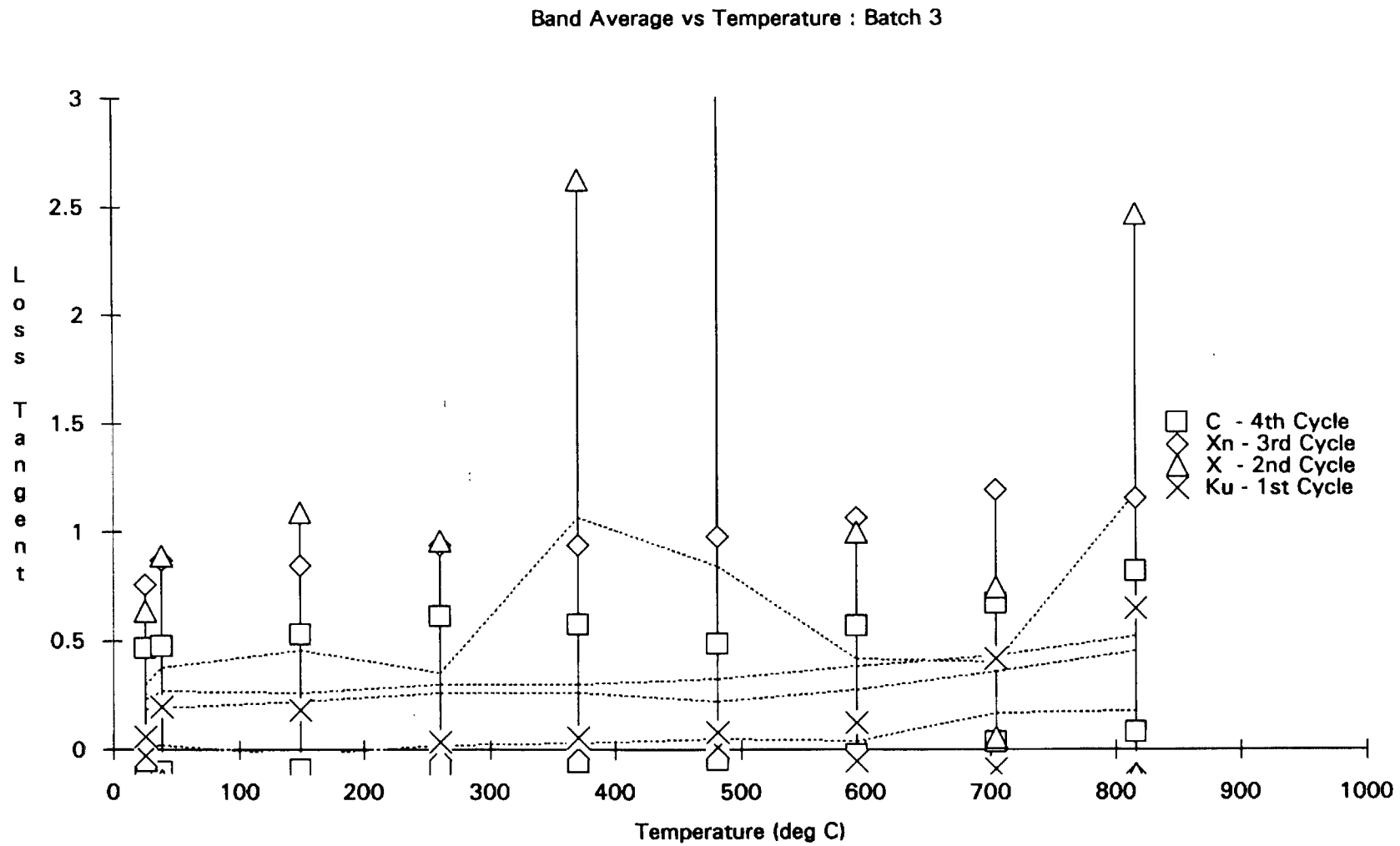

Figure 34. Average measured values with error bars for the loss tangent of samples in batch 3 through each of four heating cycles. The error bars include variations from sample to sample.

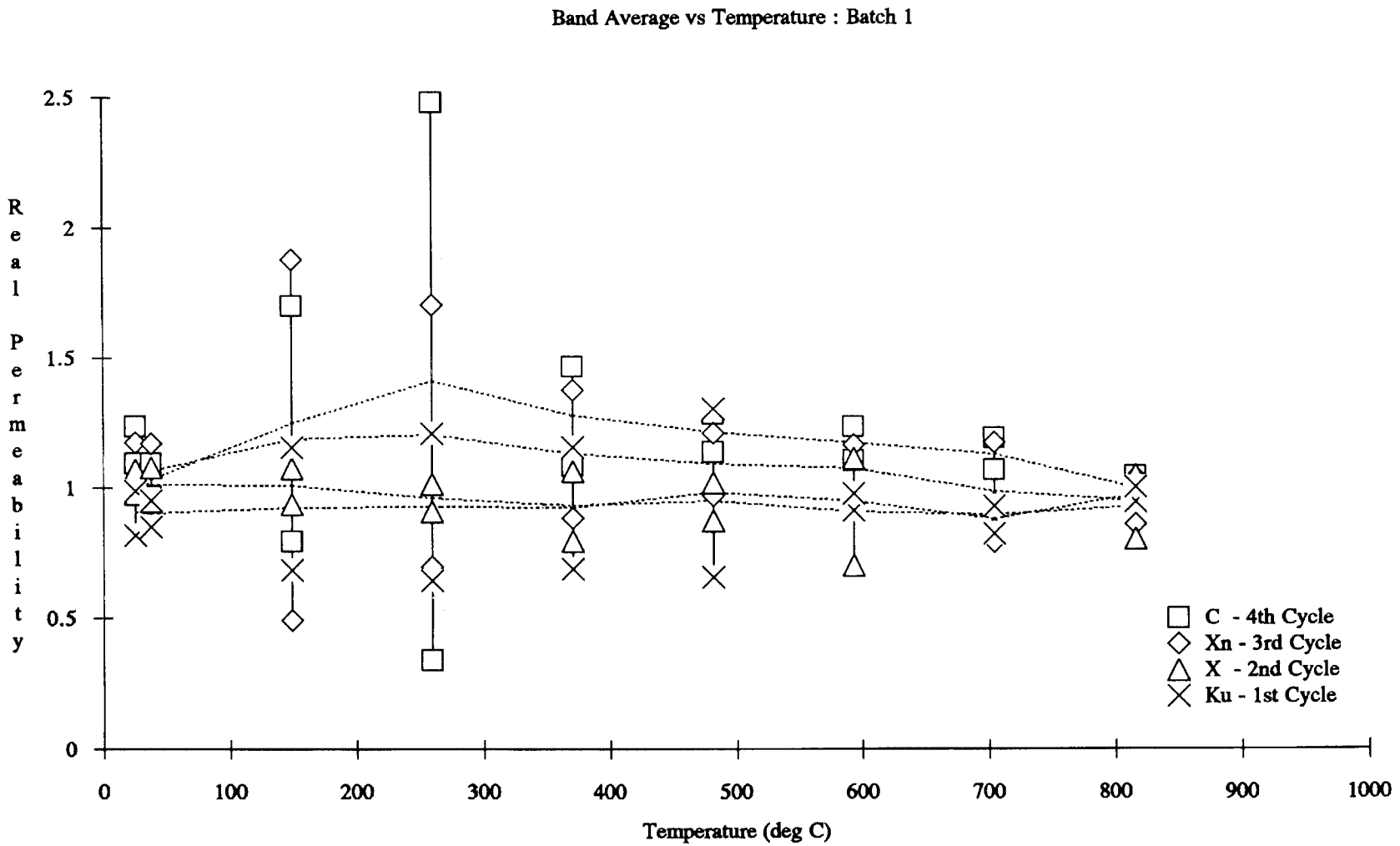

Figure 35. Average measured values with error bars for the real permeability of samples in batch 1 through each of four heating cycles. The error bars include variations from sample to sample.

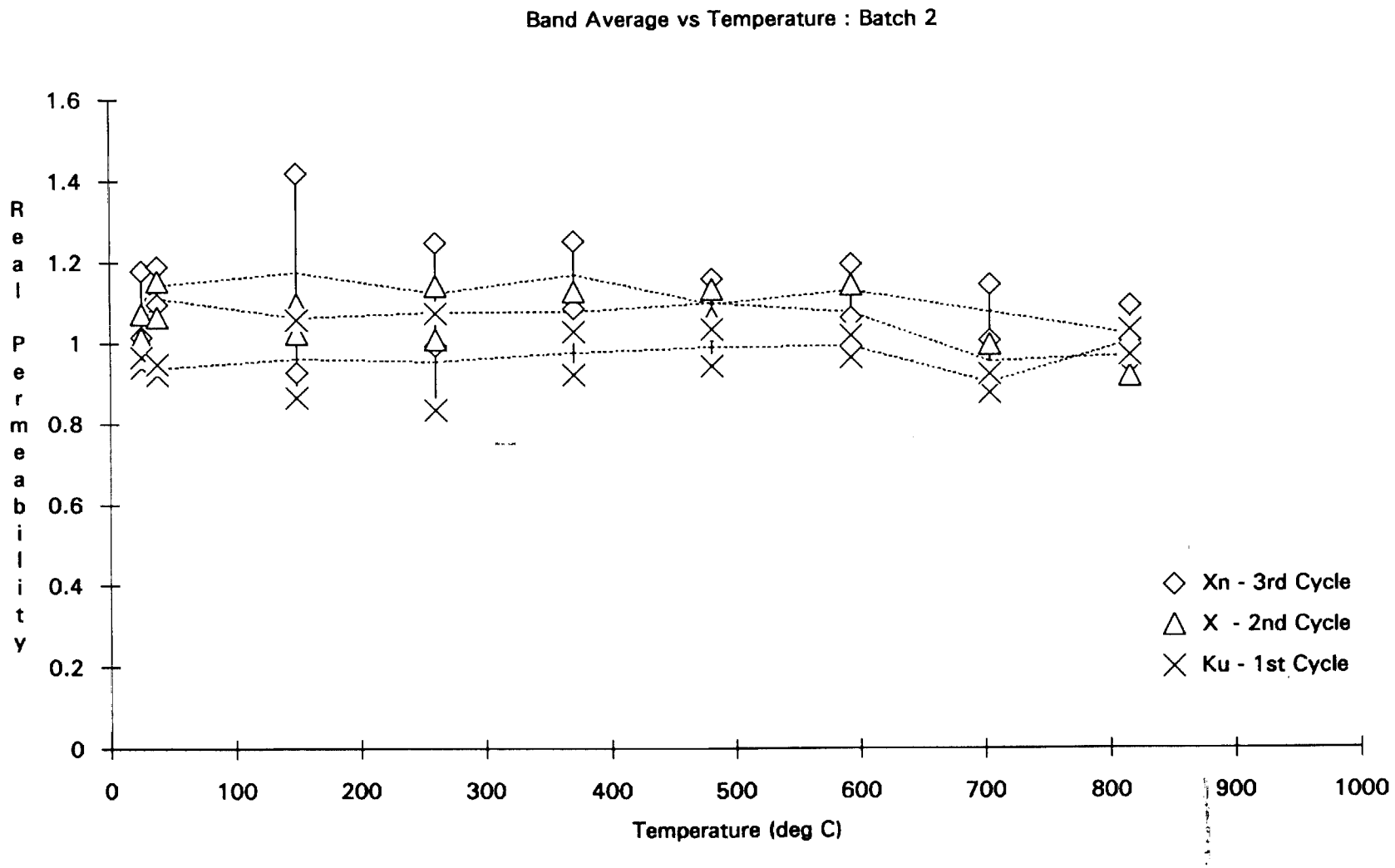

Figure 36. Average measured values with error bars for the real permeability of samples in batch 2 through each of four heating cycles. The error bars include variations form sample to sample.

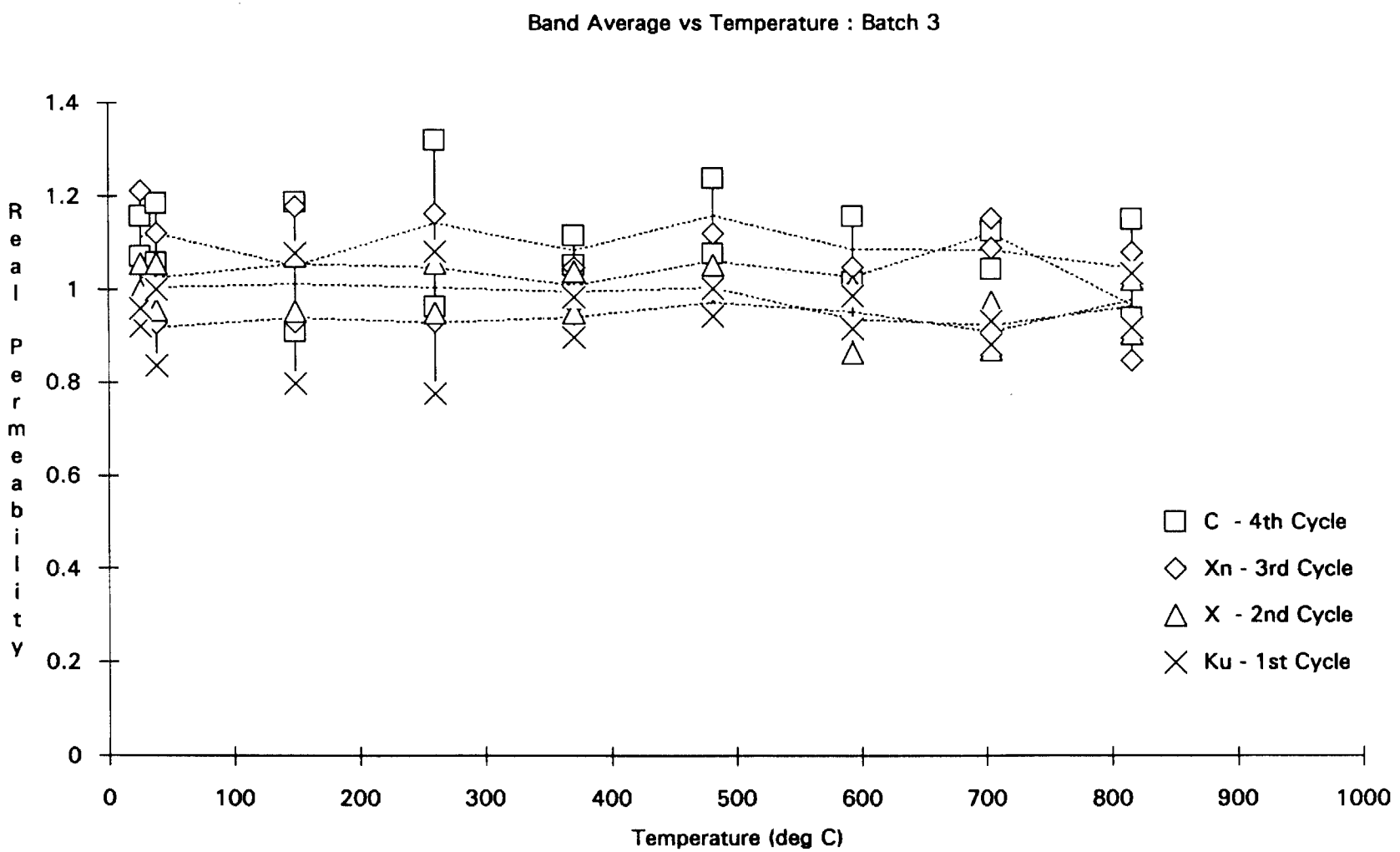

Figure 37: Average measured values with error bars for the real permeability of samples in batch 3 through each of four heating cycles. The error bars incluse variations form sample to sample.

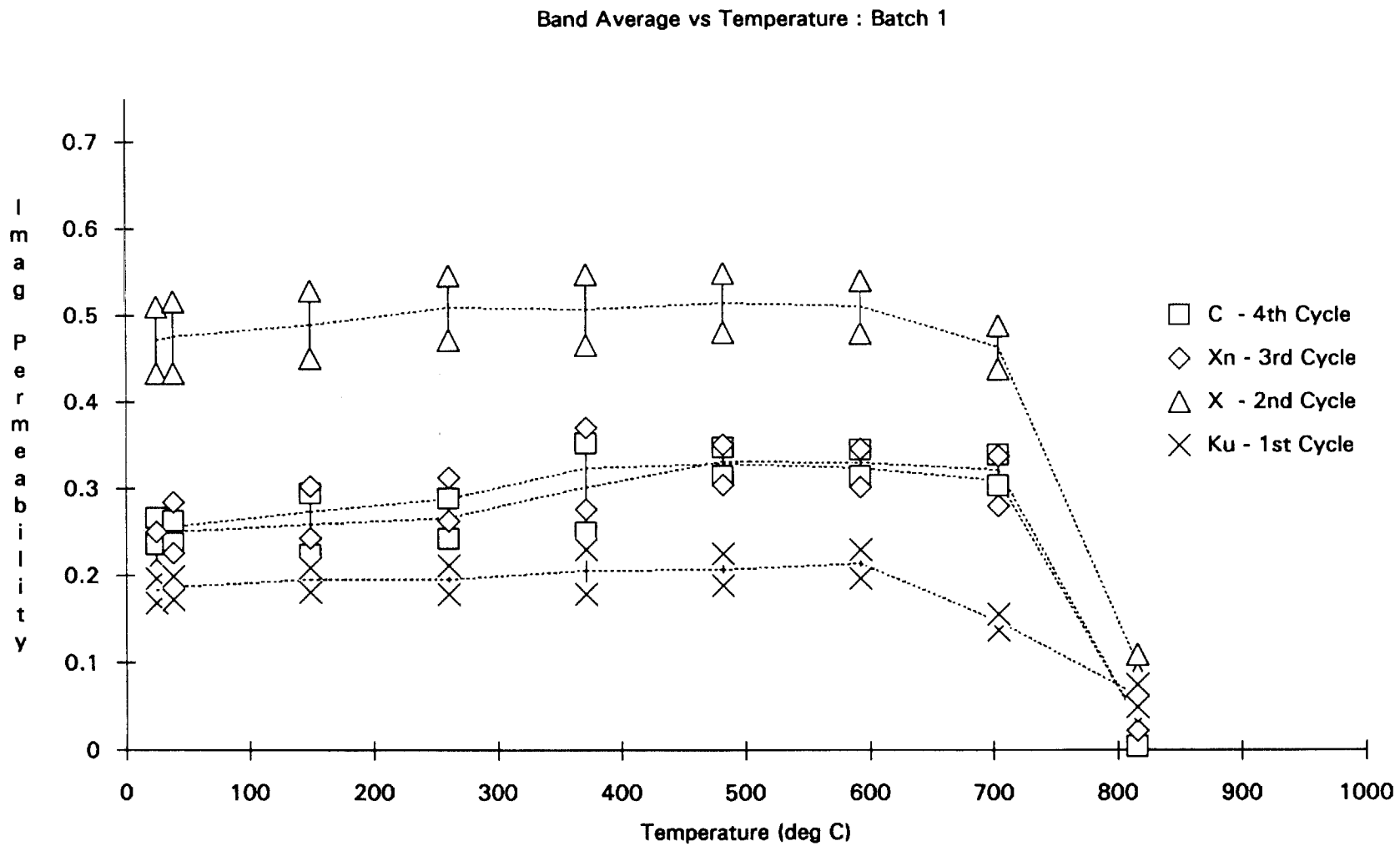

Figure 38. Average measured values with error bars for the imaginary permeability of samples in batch 1 through each of four heating cycles. The error bars include variations from sample to sample.

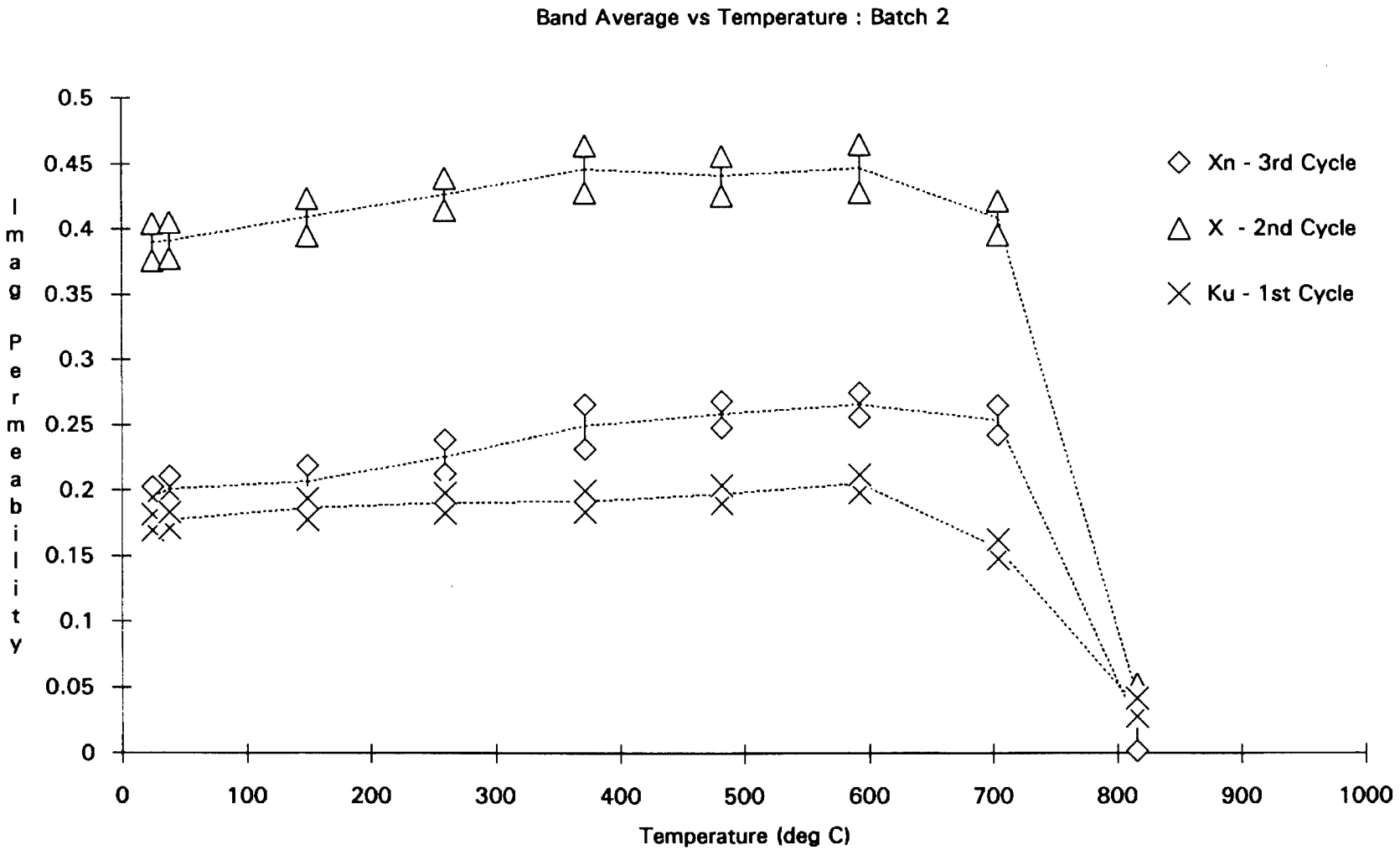

Figure 39. Average measured values with error bars for the imaginary permeability of samples in batch 2 through each of four heating cycles. The error bars include variations from sample to sample.

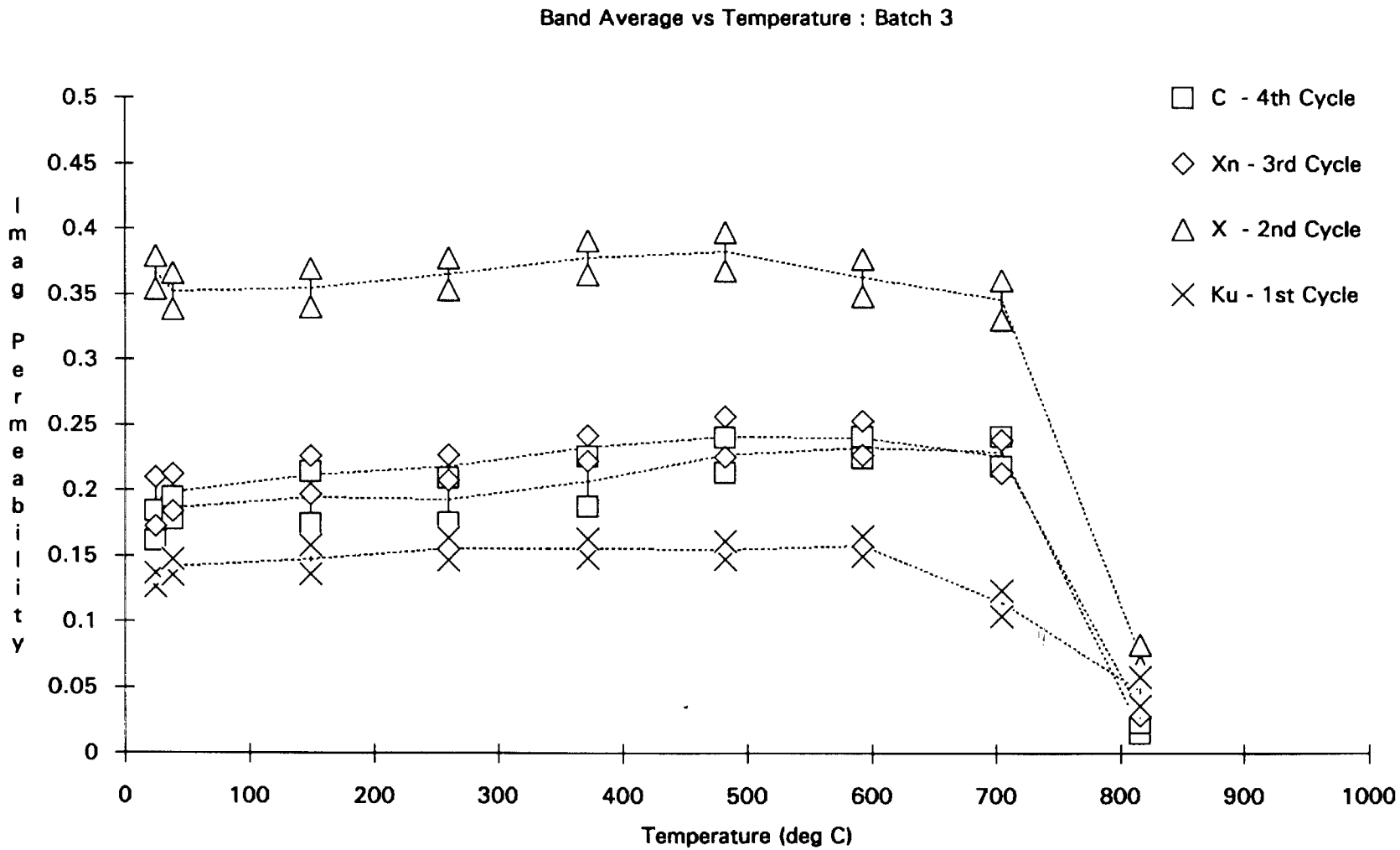

Figure 40. Average measured values with error bars for the imaginary permeability of samples in batch 3 through each of four heating cycles. The error bars include variations from sample to sample.

III. Conclusion

The waveguide cavity perturbation technique has proved useful for evaluating permittivity and permeability characteristics of NASA-supplied samples as a function of temperature. Three separate batches of samples were evaluated at temperatures of 25, 38, 149, 260, 371, 482, 593, 704, and 816°C, corresponding to 200° increments on the Fahrenheit scale up to 1500°F. These samples showed evidence of physical changes during the first two heating cycles, but appeared to stabilize during the third and fourth heating cycles. Permittivity characteristics were obviously affected by the heating. Changes in permeability due to the heating, if any, were not distinguishable. This would be consistent with expectations if one assumed that the samples consisted of ferromagnetic particulate matter suspended in a non-magnetic matrix, with the heating causing changes only in the matrix itself. It also appeared, based on measurements of different regions of each samples, that the sample bars exhibited a high degree of inhomogeneity. It would be useful to perform another series of measurements on a similar set of samples with careful monitoring and control over which region of each sample was measured at each band, in order to correlate values with regions. This would allow evaluation of the extent to which each sample did in fact exhibit inhomogeneity. Also, since the samples did not appear to be affected by the heat until the temperature rose above 600°C, it would be useful to measure all four bands through a heating cycle that ended at 600°C, then bake all samples at 816°C, and finally measure all four bands again up to 816°C. This would allow better evaluation of the effects the heating cycles had on the dielectric properties of the samples.

IV. References

1. American Society for Testing and Materials standard D 2520-86, "Complex Permittivity of Solid Electrical Insulating Materials at Microwave Frequencies and Temperatures to 1650°C."

2. American Society for Testing and Materials standard F 131-86, "Complex Dielectric Constant of Nonmetallic Magnetic Materials at Microwave Frequencies."

3. Moore, et al., "Second Order Correction in Cavity Constitutive Parameter Measurements with Application to Anisotropic Ferrites," AIP Review of Scientific Instruments, Vol. 61(3), March 1990, pp1136-42.